San Jose State University
SJSU ScholarWorks

Master's Theses | Master's Theses and Graduate Research

Summer 2017

Mobile Doppler LiDAR Observations of the Convective Boundary Layer Over California

Christopher Paul Camacho
San Jose State University

Follow this and additional works at: https://scholarworks.sjsu.edu/etd_theses

Recommended Citation
Camacho, Christopher Paul, "Mobile Doppler LiDAR Observations of the Convective Boundary Layer Over California" (2017). *Master's Theses*. 4838.
DOI: https://doi.org/10.31979/etd.rn56-a9by
https://scholarworks.sjsu.edu/etd_theses/4838

This Thesis is brought to you for free and open access by the Master's Theses and Graduate Research at SJSU ScholarWorks. It has been accepted for inclusion in Master's Theses by an authorized administrator of SJSU ScholarWorks. For more information, please contact scholarworks@sjsu.edu.

MOBILE DOPPLER LIDAR OBSERVATIONS OF THE CONVECTIVE BOUNDARY LAYER OVER CALIFORNIA

A Thesis

Presented to

The Faculty of the Department of Meteorology and Climate Science

San José State University

In Partial Fulfillment

of the Requirements for the Degree

Masters of Science

by

Christopher P. Camacho

August 2017

©2017

Christopher P. Camacho

ALL RIGHTS RESERVED

The Designated Thesis Committee Approves the Thesis Titled

MOBILE DOPPLER LIDAR OBSERVATIONS OF THE CONVECTIVE BOUNDARY LAYER OVER CALIFORNIA

by

Christopher P. Camacho

APPROVED FOR THE DEPARTMENT OF METEOROLOGY AND CLIMATE SCIENCE

SAN JOSÉ STATE UNIVERSITY

August 2017

Craig Clements, Ph.D.	Department of Meteorology and Climate Science
Neil P. Lareau, Ph.D.	Department of Meteorology and Climate Science
W. Alan Brewer, Ph.D.	National Oceanic and Atmospheric Administration

ABSTRACT

MOBILE DOPPLER LIDAR OBSERVATIONS OF THE CONVECTIVE BOUNDARY LAYER OVER CALIFORNIA

By Christopher P. Camacho

A series of transects using a truck-mounted Doppler LiDAR were conducted to obtain mobile vertical profiles of the backscatter intensity and radial velocity across California. Using the backscatter and velocity profiles, several techniques were used to estimate the depth of the convective boundary layer (CBL). The CBL was estimated from the backscatter profiles using three analyses: (1) the Haar wavelet covariance, (2) the variance, (3) the gradient. These analyses were compared to vertical velocity variance, which uses a specified threshold (0.15 $m^2 s^{-2}$) to determine CBL height. The accuracy of the backscatter analyses was heavily dependent on strong aerosol loading near the surface and clean air in the free-atmosphere. The accuracy of the vertical velocity variance was dependent on the variance threshold, and underestimated the CBL depth in conditions with weak vertical motions. The backscatter analyses tended to yield deeper CBL estimates on the order of 100 m compared to the vertical velocity variance analysis. Vertical velocity skewness and variance profiles differ between stationary and mobile observations, with variance profiles decreasing with height in cross-California transects. The Haar wavelet and vertical velocity variance techniques were applied to a transect with heavy smoke-aerosol loading emitted from a nearby wildfire. Observations show weak vertical mixing in regions with heavy smoke, along with suppressed CBL heights.

ACKNOWLEDGEMENTS

First and foremost, I would like to thank Drs. Craig Clements, Neil Lareau, and W. Alan Brewer for serving on my thesis committee. I would particularly like to thank Dr. Craig Clements for being my advisor over the past two years, and for guiding me through the whole research process. Special thanks also go out to Dr. Neil Lareau for providing key insights on processing transect data. I cannot thank Dr. Clements and Dr. Lareau enough for their feedback on this research.

I would also like to thank the faculty and the graduate students in the department of meteorology and climate science at SJSU for their support and advice with my research. I would like thank Bruno Rodríguez Queirazza in particular for his assistance in performing the series of transects.

I would finally like to thank all my friends and family. They have been a fantastic support network, and they have helped me through this process more than they would give themselves credit for.

TABLE OF CONTENTS

LIST OF FIGURES

1. Introduction

a. Review of the Planetary Boundary Layer

The evolution of the planetary boundary layer (PBL) is an important parameter for forecasters, as the PBL impacts society daily. One of the largest impacts on society is the distribution of aerosols in the PBL, and the resulting air quality. The PBL is often discussed and analyzed with respect to different regimes that occur throughout the day. Stull (1988) divides the boundary layer into three main regimes: the stable boundary layer (SBL), the residual layer (RL), and the convective boundary layer (CBL). The SBL generally forms post sunset, and is driven by radiative cooling at the surface. The radiative cooling leads to a surface based inversion, and grows in depth throughout the night. The RL lies above the SBL and is characterized by a neutral temperature profile that is topped with a capping inversion. Shortly after sunrise, convective activity near the surface leads to the development of the CBL. The CBL grows from the surface, eroding the SBL during the morning hours. The CBL is generally thought to be well-mixed, and is divided into three sections (Stull, 1988). The bottom 10% of the CBL is the surface layer, and is associated with a superadiabatic lapse rate. The mixed layer (middle 35-80%) sits above the surface layer, and often has a neutral lapse rate. The entrainment zone (top 10-60%) is located at the top of the CBL, and is associated with a capping inversion.

Over flat-homogenous terrain, the growth of the CBL is driven by upward sensible heat flux at the surface, and downward sensible heat flux in the entrainment zone. The upward surface sensible heat flux is the primary mechanism of CBL growth under clear-

sky conditions by generating a positive buoyant force. The buoyant force leads to the development of thermal eddies. These thermals are a manifestation of the turbulence generated by the positive buoyant force (Stull, 1988). The larger thermal eddies penetrate through the capping inversion, which increases the CBL depth.

b. CBL over Complex Terrain

The controls on CBL height and variability over mountainous terrain has been investigated in the literature (e.g. Banta, 1984; Kossmann et al., 1998; De Wekker et al., 2004; De Wekker and Kossmann, 2015). CBL heights typically follow four patterns along a mountain range (De Wekker and Kossmann, 2015). The first pattern is a hyper terrain following behavior of the CBL, where the CBL bulges over individual ridges and growth is limited within individual valleys. The second pattern is similar to the first, where the CBL height follows the overall terrain. Unlike the first pattern, however, the terrain following behavior is not exaggerated, with equal growth of the CBL over individual ridges and valleys. The third pattern is a uniform CBL height over the terrain, where the CBL variability is not influenced by the underlying terrain. The final pattern is contra terrain following behavior, where the CBL is suppressed over ridges and heightened over valleys.

c. Methods and platforms on determining CBL Height

The vertical extent of the boundary layer can be measured in multiple ways. Traditionally, the top of the boundary layer is determined from radiosondes using the vertical potential temperature profile (Seibert et al. 2000; Dai et al. 2014). While the gradient of the potential temperature profile diagnoses the height of the boundary layer,

the method works best during the daytime in a CBL regime. Other commonly used methods to diagnose boundary layer height analyze the turbulent kinetic energy, the Richardson number, and the vertical wind shear.

While radiosondes are the most common method for diagnosing boundary layer height, radiosondes are limited both spatially and temporally. Outside of major field campaigns, radiosondes are launched globally at 0 UTC and 12 UTC, and only provides a snapshot of the boundary layer at the time of the launch. To improve the temporal and vertical spatial resolution, other platforms are used to study the CBL including aircraft measurements.

Several studies have utilized aircraft to obtain measurements on different BL regimes (e.g. Webster and Lukas, 1992; Sellers et al., 1997; Poulos et al., 2002). These data are aggregated in Dai et al. (2014). Various methods are used in Dai et al. (2014) to derive BL heights in the SBL, CBL, and cloud-topped boundary layer (CTBL) regimes. Four commonly used methods are used to diagnose the vertical extent of the BL, including the turbulence method, the temperature gradient method, the Richardson number method (Ri), and the wind shear profile method. The turbulence method is largely based on the considerable amount of turbulence located within the BL compared to the free atmosphere (Stull, 1988). The height of the BL using the turbulence method is defined by the point at which the magnitude of the wind velocity perturbations (e.g. u', v', w') decrease the most rapidly with height. The temperature gradient method defines the top of the BL where there is a maximum in the lapse rate of the profile, indicating the presence of a strong capping inversion. The Ri method is based on the atmospheric

stability and the vertical wind shear, and the height of the BL is defined by the level at which the Ri number exceeds a set threshold value. The threshold value is an empirical value that can range from 0.15 to 0.55. The wind shear method determines BL height by the height at which the magnitude of the wind shear falls below a specified threshold. Unlike the previous methods, this method is predominantly used to determine the vertical extent of the SBL.

When applying these methods to aircraft profiles performed over land in the CBL, the temperature gradient method yielded the best results. The turbulent method yielded results similar to the temperature gradient method, with a correlation coefficient of 0.93 over the analyzed profiles. The Ri number method performed poorly at determining the depth of the CBL, and was suggested as an inaccurate method at estimating CBL heights. While aircraft can provide high resolution in-situ measurements that can be used to estimate CBL heights, aircraft platforms are expensive and potentially require a large crew. In addition, aircraft cannot sample continuously over a large period of time due to fuel constraints. To obtain high temporal observations on the CBL, remote sensing instrumentation is often utilized.

Remote sensing platforms such as Sound Detection and Ranging (SODAR) and Light Detection and Ranging (LiDAR) platforms have been used to study CBL evolution (e.g. Beyrich, 1995; Tucker et al., 2009). Both platforms have the capability of running remotely and continuously, allowing for detailed observations on the CBL. While both platforms provide high temporal and vertical resolution measurements, both suffer from blind spots in the lowest range gates. This blind spot can potentially limit the platform's

capability in estimating the BL height in certain situations, such as in the presence of a shallow stable boundary layer (Seibert et al., 2000). In addition, the environment the platforms operate can influence the quality of the data. Environmental noise can create artifacts within SODAR data (Crescenti, 1998), but advances in signal processing reduce the impact of environmental noises. In addition, the depth of the CBL may exceed the operating range of the SODAR (Beyrich, 1995). Most LiDARs are dependent on the aerosol concentrations in the atmosphere. Aerosol LiDARs yield limited returns in clean air environments, and the beam will also attenuate on large particles (e.g. water droplets). For most situations, both platforms provide a feasible means to observe the CBL height.

LiDARs, unlike SODARs, can be utilized for mobile applications due to their greater portability. Various field campaigns have utilized airborne LiDARs to analyze CBL spatial variability (Carroll, 1989; McElroy and Smith, 1991; Nyeki et al., 2000; Nyeki et al., 2002; Reitebuch et al., 2003; De Wekker et al., 2004; Weissmann et al., 2005; De Wekker et al., 2012), the majority of which relied on an aerosol LiDAR. A couple of studies assumed the top of the aerosol layer, the level at which aerosol loading rapidly decreases, was the top of the CBL (Nyeki et al., 2000, 2002). Further investigation in De Wekker et al. (2004) showed via numerical simulations that CBL heights are frequently lower than the aerosol layer (AL) heights, particularly in mountainous regions. In De Wekker et al. (2004), the AL that remains rather uniform over a mountain range, and largely does not follow the terrain. The estimated CBL heights show the CBL following the terrain, unlike the AL. Other studies suggest the CBL will closely follow the terrain during the morning, but will continue to grow throughout the day, leaving a uniform CBL

height over mountainous terrain (Kossman et al., 1998). CBL growth within valleys must exceed the CBL growth at individual ridges for the development of a uniform CBL height (De Wekker and Kossmann, 2015). This scenario is most likely to occur during the summer on days with strong surface heating and weak morning inversions.

Although the CBL spatial variability has been analyzed using airborne aerosol LiDARs, relatively few studies have used a Doppler LiDAR for mobile observations. Carroll (1989), Reitebuch et al. (2003), Weissmann et al. (2005), and De Wekker et al. (2012) are a handful of studies that implemented an aircraft Doppler LiDAR. While these studies made observations with a Doppler LiDAR, the primary focus was on the horizontal wind fields related to sea breezes in complex terrain, or flow around a mountain range. The CBL height variability is largely not addressed in these studies, or is not discussed in great detail or length. The one exception is Weissmann et al. (2005), who explicitly discusses the vertical velocities measured by the LiDAR, but did not attempt at estimating CBL heights from the measured vertical velocities. The vertical velocities measured by a Doppler LiDAR would allow for a direct determination of the CBL, and would eliminate the need for numerical analysis to estimate CBL variability.

d. Smoke impacts on CBL evolution

The growth of the CBL has been studied in detail under clear skies and fair weather. Investigations into how the PBL reacts during anomalous conditions, such as when shaded by smoke from wildfires, have received little attention in comparison. In 2016, wildfires across the United States burned roughly 2.2 million hectares. While the smoke emissions vary for each incident, the smoke adversely impacts the air quality of the

immediate and downwind regions. Due to the high albedo of smoke, incoming solar radiation is either scattered or absorbed, decreasing the amount incident at the surface.

Robock (1988) was one of the first studies to investigate the impact smoke from wildfires have on the CBL, with focus on the influence on surface temperatures. The temperatures from several weather stations in mountainous terrain of northern California and southern Oregon were analyzed during a significant smoke event. These data show suppressed daytime temperatures up to 15°C compared to the climatological mean. Robock (1988) suggests the decreased heating at the surface leads to a feedback mechanism that prolongs the length of the nocturnal inversion. The combination of increased stability and decreased solar radiation at the surface likely limits CBL growth.

More recent studies, such as Lareau and Clements (2014), also observe suppressed surface temperatures in smoke laden regions. In their study, Lareau and Clements observe a 3°C decrease in the ambient temperature as a smoke layer passed over the observation location. This scenario is unique, however, as the decrease in temperature was related to a density current generated by the smoke. Therefore, it is unclear if the temperature decrease was driven solely by the smoke, or was influenced by other advective properties.

Attempts have been made at quantitatively estimating the smoke radiative impacts of smoke on the environmental lapse rate. Specialized numerical models, such as the Regional Atmospheric Modeling System coupled with the Assimilation and Radiation Online Modeling of Aerosols (RAMS-AROMA), have been used to diagnose this question. Wang and Christopher (2006) simulates smoke transport from biomass

burnings in Central America over the southeastern United States using RAMS-AROMA to investigate the impacts on the CBL. In their study, the transported smoke was diffuse with the aerosol optical thickness (AOT) half compared to that of the source region. While the AOT of smoke plumes is commonly discussed, it is important to keep in mind the radiative effects on the downward shortwave radiation are not entirely proportional to the change in AOT. Wang and Christopher (2006) argues this is primarily due to the importance the solar zenith angle, surface characteristics, and the vertical aerosol distribution have on incident shortwave radiation. Even with a relatively diffuse smoke layer, the radiative effects impact the 2m surface temperatures as well as the lapse rate in the CBL. The smoke layer suppressed the overall diurnal temperature cycle, and reduced the daily maximum and minimum temperatures. In addition, the radiation absorbed by the smoke layer increased the lapse rate within the CBL.

Using a truck mounted Doppler LiDAR with a vertically pointing scan, detailed observations of the CBL variability were conducted over flat and mountainous terrain. Rather than relying on numerical simulations to estimate the CBL height variability, the height of the CBL was directly calculated using the observed vertical velocities. With these data and mobile platform, smoke layer impacts on the CBL structure can be observed.

2. Methodology

a. Mobile Platform

The California State University Mobile Atmospheric Profiling System (CSU-MAPS) provides novel mobile observations on the boundary layer. CSU-MAPS consists of two primary platforms: (1) a deployable 32-m micrometeorology tower, and (2) a modified 4x4 truck equipped with remote sensing and in-situ instrumentation (Clements and Oliphant, 2014). The truck (Fig. 1) was the only platform implemented in this study, and hereafter is the only platform referenced when discussing CSU-MAPS. CSU-MAPS is equipped with a CS-215 temperature-relative humidity probe, and an RM Young 5103 prop anemometer, each with a 1 Hz sampling frequency and 1 min averaging period. In addition, a GRAWMET radiosonde system is integrated into CSU-MAPS, allowing for unique in situ atmospheric profiles in remote locations. A Garmin GPS tracked the positioning, altitude, and speed of the platform when mobile.

A Halo Photonics Doppler LiDAR is mounted in the bed of CSU-MAPS on an airbag frame, and is an integral part of the platform. The LiDAR provides high spatial and temporal resolution observations of the atmosphere, and has a maximum range of 9600-m. Several different continuous scanning modes are supported by the LiDAR, including a range height indicator (RHI), plan position indicator (PPI), and zenith stare scans. The LiDAR was configured to have an 18-m range gate resolution with 1Hz resolution. The laser emitted by the LiDAR has a wavelength of 1.5 μm, making the laser eye safe unlike some other LiDARs that operate in the UV or visible spectrum.

Fig. 1. CSU-MAPS as discussed in this paper. The LiDAR (a) is mounted in the bed of CSU-MAPS, with the in-situ instrumentation (b) mounted to the right.

The LiDAR returns profiles of the backscatter intensity (m^{-1} Sr^{-1}) and the radial velocity (m s^{-1}) per range gate. Additional information on the signal-to-noise ratio (SNR) is also recorded, which helps discriminate between real observations and instrument noise. The aerosol loading in the atmosphere is correlated with the backscatter intensity and the SNR to an extent (Bozier et al., 2007; Pearson et al., 2009). In clean air environments, a low SNR is observed and is associated with noisier returns in the radial velocity and backscatter intensity. The optimum atmospheric environment for the LiDAR contains aerosols with diameters near the wavelength of the laser or smaller. Any particles significantly larger than the wavelength and in sufficient concentration, such as cloud droplets, fully attenuate the beam.

When CSU-MAPS deploys during various field campaigns, the LiDAR is set into a zenith stare scan, allowing for mobile observations of the vertical velocity and

backscatter intensity. These transects provide high resolution data that capture the spatial variability of the two fields over various terrain and geographical transects.

b. Mobile Data Correction

To obtain observations on the true vertical motions in the atmosphere, the LiDAR must remain perfectly level. During mobile transects, however, the instrument seldom remains perfectly level. Doppler LiDARs operating over the oceans, either on buoys or sea-containers (seatainers), suffer from similar bias. In such scenarios, the data are corrected to account for motion induced from waves by using the angular rate recorded by inertial devices integrated into the platforms (Hill et al., 2008). The LiDAR mounted on CSU-MAPS contains an onboard accelerometer that records the pitch and roll for each observation, but not the angular rate. Using the recorded pitch (α) and roll (β) to calculate the zenith angle offset (γ), the observed velocity is corrected to obtain an improved estimate on the true vertical velocity.

To calculate the zenith offset, tilted unit vectors were created from a fixed frame of reference (Fig. 2). The unit vectors were scaled and normalized with respect to the largest angle deviation, whether it is pitch or roll. For instance, with a 10° roll and a 5° pitch the roll unit vector ($\hat{R}$) will have a magnitude of 1 and the pitch unit vector ($\hat{P}$) will have a magnitude of 0.5. The pitch and roll unit vectors are projected onto their respective axes which are assigned as the X-axis for pitch and the Y-axis for roll:

$$\vec{P}_x = \hat{P} \cdot \cos\alpha \quad , \tag{1}$$

$$\vec{R}_y = \hat{R} \cdot \cos\beta \quad , \tag{2}$$

where $\vec{P}_x$ and $\vec{R}_y$ are the projected normalized vectors. $\hat{P}$ and $\hat{R}$ are added together to create a three-dimensional vector, $\overrightarrow{PR}$:

$$\overrightarrow{PR} = \hat{P} + \hat{R} \quad , \tag{3}$$

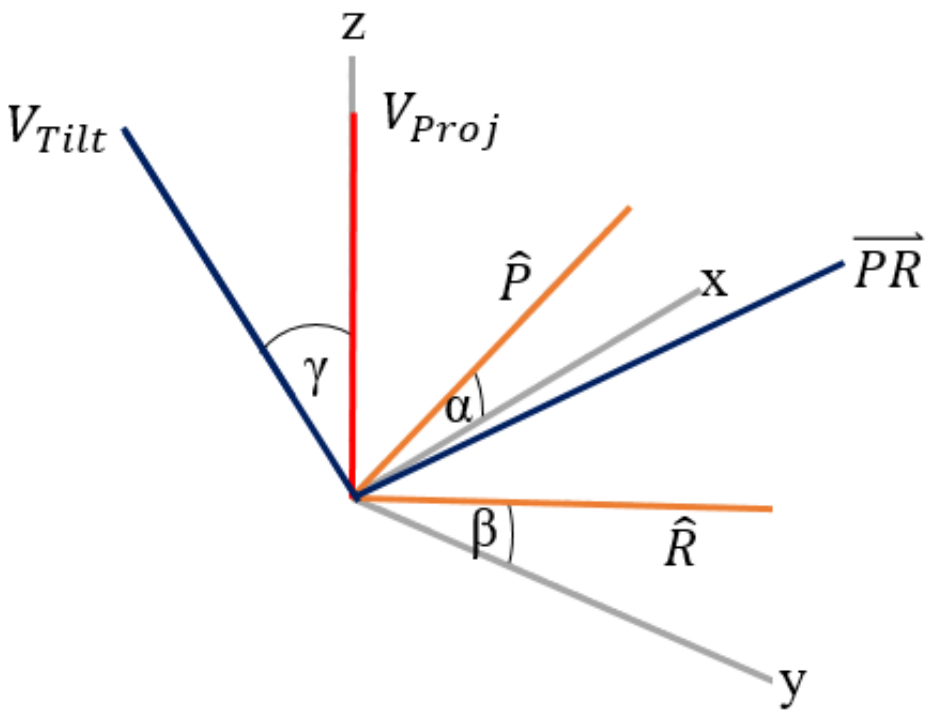

Fig. 2. The 3-D representation of the titled frame to the fixed reference frame. The pitch and roll angles in this example are the same, resulting in same sized pitch and roll vectors.

The same is done with $\vec{P}_x$ and $\vec{R}_y$, which is the projection of $\overrightarrow{PR}$ onto the XY-plane ($\overrightarrow{PR}_{xy}$):

$$\overrightarrow{PR}_{xy} = \vec{P}_x + \vec{R}_y \quad , \tag{4}$$

Taking the inverse cosine of $\overrightarrow{PR}$ and $\overrightarrow{PR}_{xy}$ yields the zenith offset (γ):

$$\gamma = \cos^{-1}\left(\frac{\left|\overrightarrow{PR}_{xy}\right|}{\left|\overrightarrow{PR}\right|}\right) \quad , \tag{5}$$

Using γ, the tilted velocity vector (V_{Tilt}) can be projected onto the Z-axis, providing the vertical component of the observed radial wind (V_{Proj}):

$$V_{Proj} = V_{Tilt} \cdot \cos\gamma \quad , \tag{6}$$

To further improve the vertical velocity estimate, an external triaxle accelerometer was mounted on the LiDAR. The accelerometer records the instantaneous accelerations along the X, Y, and Z axes, allowing for the correction of vertical velocities induced by the jostling of the truck while driving over a rough road. The accelerometer was mounted near the head of the LiDAR, and was synced with the LiDAR. The accelerometer recorded the linear accelerations at 100 Hz. The influence of gravity along the Z-axis resulted in an observed acceleration of 9.8 m s^{-2}, even while the platform was at rest. To remove this bias, a high pass filter was applied to the observed vertical accelerations. Using the bias corrected accelerations, the data were integrated to obtain 1 Hz measurements. These integrated data, when multiplied by a time-step of 1 s, have units of m s^{-1} and can be used to correct the vertical velocities as observed by the LiDAR.

The velocity of CSU-MAPS can also be taken into consideration when correcting the mobile data, similar to correction of airborne radar. Where radar data has up to nine degrees of freedom including the aircraft groundspeed, drift angle, pitch, roll, vertical velocity, radar pitch and tilt, and the radar range delay (Lee et al., 1994; Bosart et al., 2002), the degrees of freedom are reduced with CSU-MAPS. Since the vertical velocity is the only variable observed with CSU-MAPS, the drift angle does not have an influence

and is therefore neglected. The range delay error does not influence Doppler velocities (Bosart et al., 2002), and is also neglected. In addition, the pitch and tilt of CSU-MAPS are assumed to be the same as the LiDAR. This reduces the number of influential variables from nine to four: (1) the groundspeed of CSU-MAPS, (2) LiDAR pitch, (3) LiDAR roll, and (4) the vertical velocity. The correction of variables 2-4 were discussed in the previous paragraphs, leaving the groundspeed correction.

The speed of CSU-MAPS was tracked by the onboard GPS, and was recorded in one minute averages. Normally the pitch angle aligns with the direction of travel, but due to the mounting of the LiDAR on CSU-MAPS, the roll angle aligns with the direction of travel. The added vertical velocity induced by the roll angle (θ) is defined as:

$$\Delta V = V_T \cdot sin(\theta), \tag{7}$$

Where ΔV is the projection of the platform velocity into the vertical, V_T is the platform velocity, and θ is the pitch of the lidar into the direction of motion. Subtracting ΔV from the observed vertical velocities yields the motion corrected velocities. While the vertical velocities induced by the groundspeed can be backed out, uncertainty remains on the contamination of cross-wind flow into the vertical from the pitch offset. Figure 3 shows an example of the pitch and roll distributions from a mobile transect, as well as the integrated linear velocities derived from the external accelerometer.

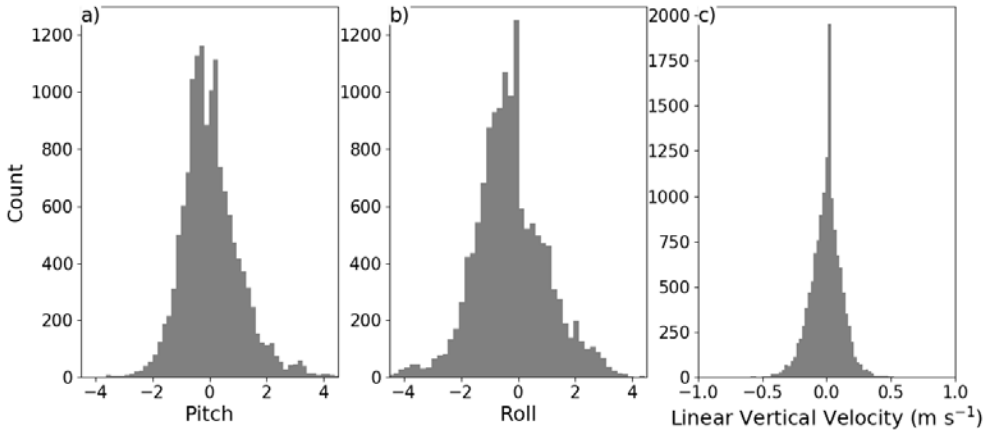

Fig. 3. Typical values of pitch (a), roll (b) in degrees, and linear vertical velocities (c) during a transect. The linear vertical velocities are derived from the external accelerometer.

c. Determination of CBL Heights

Using the motion corrected data, the CBL depth can be estimated along a given transect. Numerous methods have been used to determine the height of the CBL, which vary in complexity. Early methods simply analyze the vertical gradient of backscatter, searching for a minimum in the gradient (Endlich et al., 1979). The minimum indicates a rapid drop off in aerosol concentrations associated with the top of the CBL. Other simplistic methods specify the top of the CBL where aerosol backscatter returns drop below a set critical threshold (Melfi et al., 1985). Improvements to the gradient method have been made, with more recent studies integrating a Haar wavelet with the backscatter profile to calculate the Haar wavelet covariance (Ware et al., 2016). The Haar wavelet covariance is defined as:

$$w(z) = \frac{1}{d}\int dz' \beta H(z, z', d) \quad , \tag{8}$$

$$H(z,z',d) = \begin{cases} 1 & z - d/2 < z' < z \\ -1 & z < z' < z + d/2 \\ 0 & |z' - z| > d/2 \end{cases}, \quad (9)$$

Where $H(z,z',d)$ is the Haar wavelet of width d centered at height z, $z'$are the range gates, and β is the backscatter intensity. The maximum of this profile indicates the top of the CBL.

The variance method is another technique at estimating the CBL depth, and is based on analyzing the backscatter variance profiles. The CBL top is associated with a maximum in the variance profile (Hooper and Eloranta, 1986; Piironen and Eloranta, 1995; Menut et al., 1999).

A challenging obstacle in using backscatter profiles to diagnose CBL depth is preventing the algorithms from detecting an elevated aersosol layer (AL). The algorithms detecting an elevated AL would result in an overestimation of the CBL depth. Ware et al. (2016) includes safeguards such as ensuring the growth of the CBL does not exceed a set rate, which was set to 100 m min^{-1}.

The variance method can be adapted to the observed vertical velocities to diagnose the CBL depth. Such analysis has been performed on stationary or ship-based Doppler LiDARs (Banta et al., 2006; Tucker et al., 2009), where the CBL top is defined by the level where the vertical velocity variance drops below a pre-defined threshold. Tucker et al. (2009) calculated the variance in 15 minute windows with a threshold of 0.04 m^2s^{-2}, but states the threshold is sensitive depending on the location. The sensitivity of the threshold varies compared to over the ocean vs over land. When calculating the variance, Tucker et al. (2009) filters out erroneous returns as the result of instrument noise, which

tends to increase with low SNR values. In this study, the data were filtered with an SNR threshold of 1.015, which removes data points potentially biased with instrument noise. While this filter does not address or remove instrument noise in radial velocities with high SNR values, it helps prevent the CBL from being overestimated due to noisy data. Comparisons between the variance derived CBL tops to those from radiosonde observations yield similar estimates, with a correlation coefficient of 0.91 in Tucker et al. (2009).

Another useful quantity for analyzing the structure of the boundary layer is the vertical velocity skewness, which is defined as:

$$s = \frac{\overline{w'^3}}{\overline{w'^2}^{3/2}} \quad , \tag{10}$$

where $\overline{w'}$ are the vertical velocity perturbations within a set averaging window. Under clear sky conditions, the skewness profile within the CBL is typically positive and increases with height (Hogan et al., 2009). This profile indicates updrafts within the CBL are often more narrow and greater in magnitude compared to the downdrafts. This signifies that vertical motions and turbulence in the CBL are predominantly driven by surface heating. Under a cloud-topped BL, vertical motions are largely driven by radiative cooling near the cloud top, resulting in stronger, more narrow downdrafts compared to the updrafts in the CBL. These downdrafts lead to negative skewness values throughout the upper portion of the CBL. The entire skewness profile will not be negative, as surface heating leads to positive values (Moyer and Young, 1990; Hogan et al., 2009).

In this study, the methodology outlined by Tucker et al. (2009) and Ware et al. (2016) to derive the CBL depth along a transect was closely followed. The backscatter gradient and variance methods were also used to estimate the CBL depth for extra comparison. The Haar wavelet, backscatter gradient, and backscatter variance methods will hereafter be referred to as the backscatter analyses.

The aforementioned studies base their CBL determination algorithms from a temporal perspective. Due to the mobile nature of these data in this study, however, a spatial perspective is adopted. Instead of setting the statistical averaging windows to an n-minute period, averaging windows were created with respect to distance traveled (a 1-km window throughout the study). The 1-km windows helped ensure an adequate amount of thermals were sampled for the vertical velocity variance analysis. When determining the CBL height using the vertical velocity variance, a threshold value of 0.15 $m^2 s^{-2}$ was implemented. The threshold is sensitive to the strength of the vertical velocities, and may not yield the best results in conditions with weak vertical velocities. While the 0.15 $m^2 s^{-2}$ may not be sensitive enough for weaker vertical velocities, the threshold tended to prevent the detection of gravity waves within elevated aerosol layers, which prevented an overestimation of the CBL. A CBL growth filter is also implemented on the backscatter analyses to prevent the detection of an elevated aerosol layer. The bounded growth filter was slightly less stringent than the filter in Ware et al. (2016), with CBL growth limited to 200 m km^{-1} (translating to 400 m min^{-1} when traveling at 30 m s^{-1}). A less stringent filter was used due to the high variability of the AL observed while mobile. The

backscatter analyses are conducted on the entirety of the data, regardless if only one section is the focus.

d. Mobile Transects

A series of cross-California transects from San Jose, CA to Reno, NV (Fig. 4) were conducted during August through October in 2016. A total of eight transects were conducted in this time frame with the following dates: 22 Aug 2016, 24 Aug 2016, 9 Sep 2016, 10 Sep 2016, 23 Sep 2016, 17 Oct 2016, and 25 Oct 2016. In this study, only the transects conducted during August and September were analyzed, due to the favorable weather and timing of the transects in studying the CBL under clear and calm conditions. Apart from 23 Sep 2016, a single transect was conducted on each day departing from either San Jose or Reno. Two transects occurred on 23 Sep 2016, departing San Jose in the early morning, and returning in the late evening.

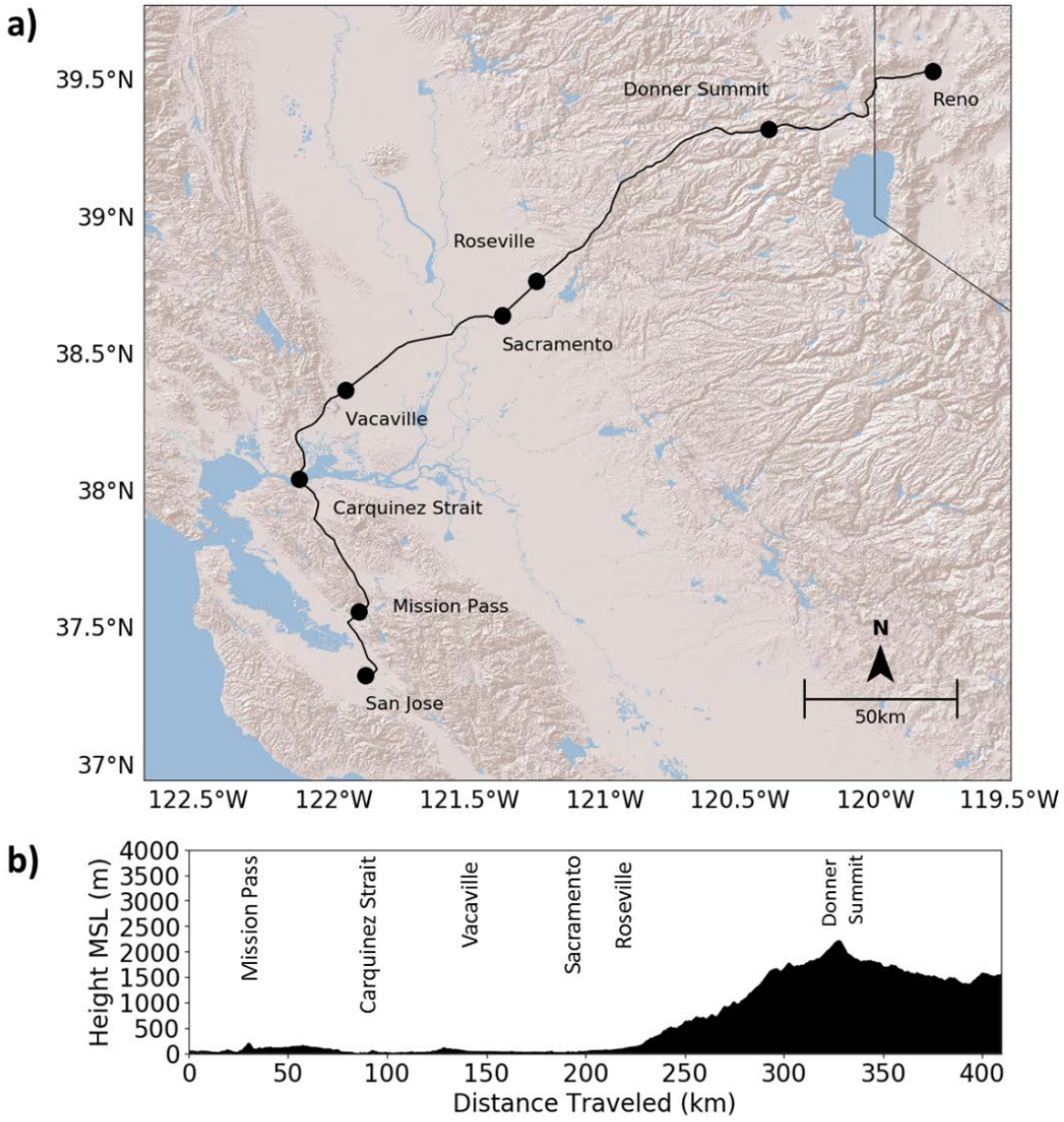

Fig. 2. Map of the cross-California transect route from San Jose, CA through Reno, NV (a), and the vertical topographic cross section of the transect (b).

The transects were divided into the three separate sections: (1) San Jose, CA – Vacaville, CA, representing the transect through the California Bay Area, (2) Vacaville, CA – Roseville, CA, representing California's Central Valley, and (3) Roseville, CA – Reno, NV, representing the transition from the Central Valley to the Sierra Nevada. Using these sections, the CBL and AL spatial and temporal variability were compared across California. To prevent an initial detection of an elevated AL, backscatter profiles from each transect were analyzed using San Jose as the origin. The backscatter intensity in the boundary layer around San Jose generally exceeds the backscatter intensity of any elevated ALs. As a result, the chance of the backscatter analyses detecting an elevated AL at the beginning of a transect is reduced. Transects starting at Reno do not always have sufficient backscatter intensity in the boundary layer, and may default to detecting an elevated AL if one is present.

One question that arises while analyzing the observed vertical velocities while mobile are the artificial velocities induced by CSU-MAPS while driving over rough terrain and roads. To address this question, a test transect was conducted on the afternoon of 15 June 2017. The transect consisted of a stationary section and a mobile section. CSU-MAPS sat stationary for a continuous 2 hours then drove around for 45 minutes. This test transect shows how a mobile platform impacts the vertical velocity measurements.

The final section of this paper will focus on a case study of how smoke from a large wildfire impacted the CBL. Using the same methodology from the cross-California transects, observations on the CBL variability in a smoke-heavy environment are presented.

3. Results

a. Synoptic Conditions, Transect Overview, and Error Analysis

The entire backscatter intensity and vertical velocity profiles along the six transects are shown in Figs 5 and 6, respectively. The transects in this study were conducted during clear sky conditions, except for the mornings of 22 Aug 2016 and 9 Sep 2016, as a marine layer stratus was present during the beginning portion of the transects. The 500hPa geopotential heights during these transects are shown in Fig. 7. The majority of the transects were conducted under weak geopotential height gradients, except for 23 Sep, which was associated with a passing trough generating stronger northwesterly flow aloft. The passing trough may partly be responsible for the clear air observed in the central valley on the morning of 23 Sep 2016. The passing trough likely advected any elevated aerosol layers, or residual layers, out of the Sacramento area.

All transects showed a well-defined AL in the Santa Clara Valley (San Jose – Mission Pass), regardless of the time of day. Backscatter returns tend to largely dissipate upon exiting the valley, but the AL is still generally discernable. Multiple transects showed decreasing backscatter returns through the East Bay until Vacaville. Backscatter returns tend to increase upon entering the Central Valley, resulting in a well-defined AL.

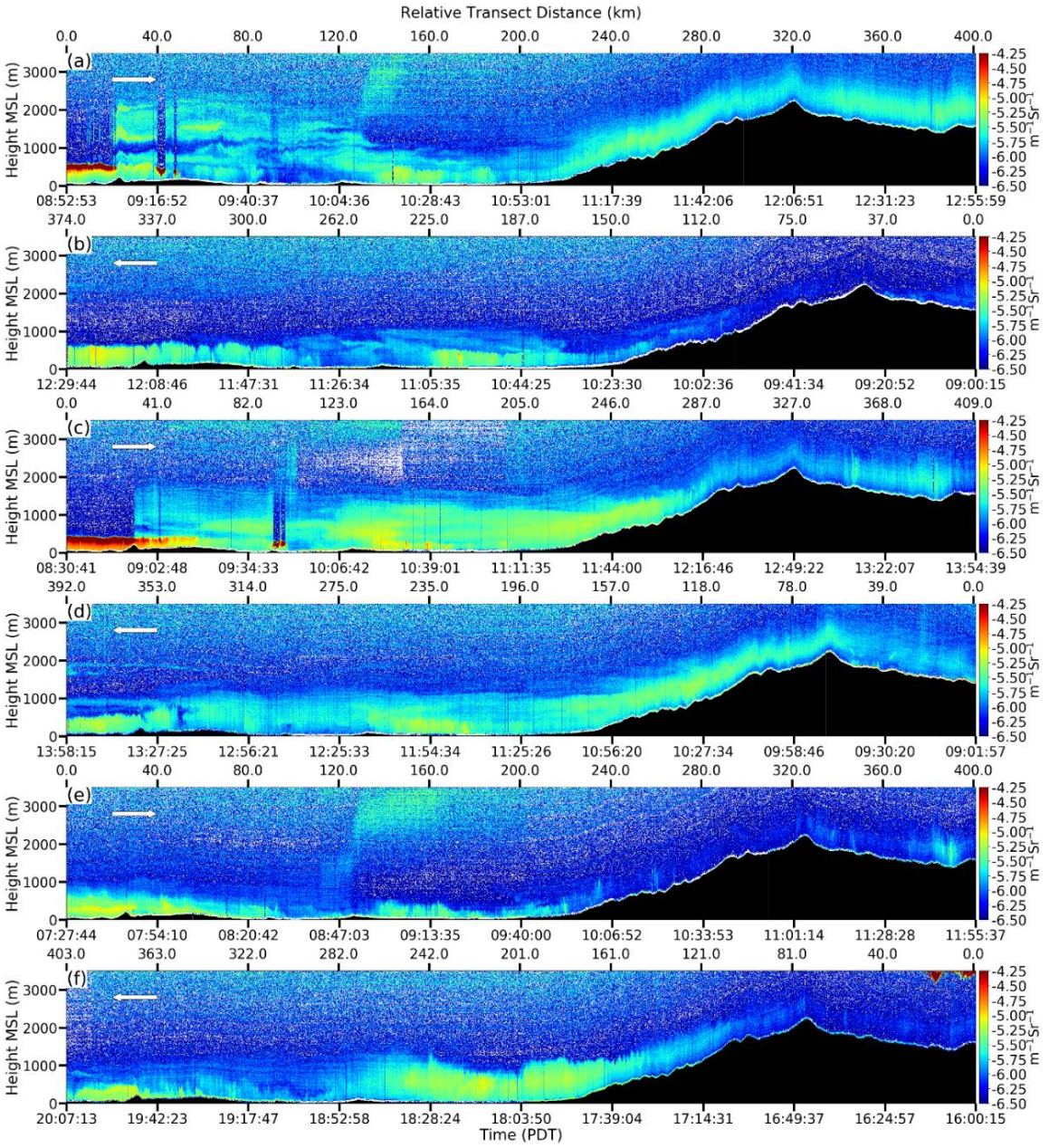

Fig. 3. The backscatter intensity profiles across the six transects: (a) 22 Aug 2016, (b) 24 Aug 2016, (c) 9 Sep 2016, (d) 10 Sep 2016, (e) morning 23 Sep 2016, (f) afternoon 23 Sep 2016. The arrow in the upper left corner denotes the direction of travel. The bottom axis displays the time of the transect, and the top displays distance traveled.

The presence of an AL over the Sierra Nevada was largely variable. Certain days had a consistent AL across the mountain (e.g. Fig. 5a), and others either had a partially developed or a non-existent AL (e.g. 5b and 5e). Days with light aerosol loading over the Sierra Nevada proved a challenge to quantitatively measure the CBL variability, as there were noisy and limited returns. Due to the limited returns, discussion on the CBL structure over the Sierra Nevada on 24 Aug 2016, and the morning of 23 Sep 2016 is omitted. The following sections will focus in greater detail on the three main sections of the transects.

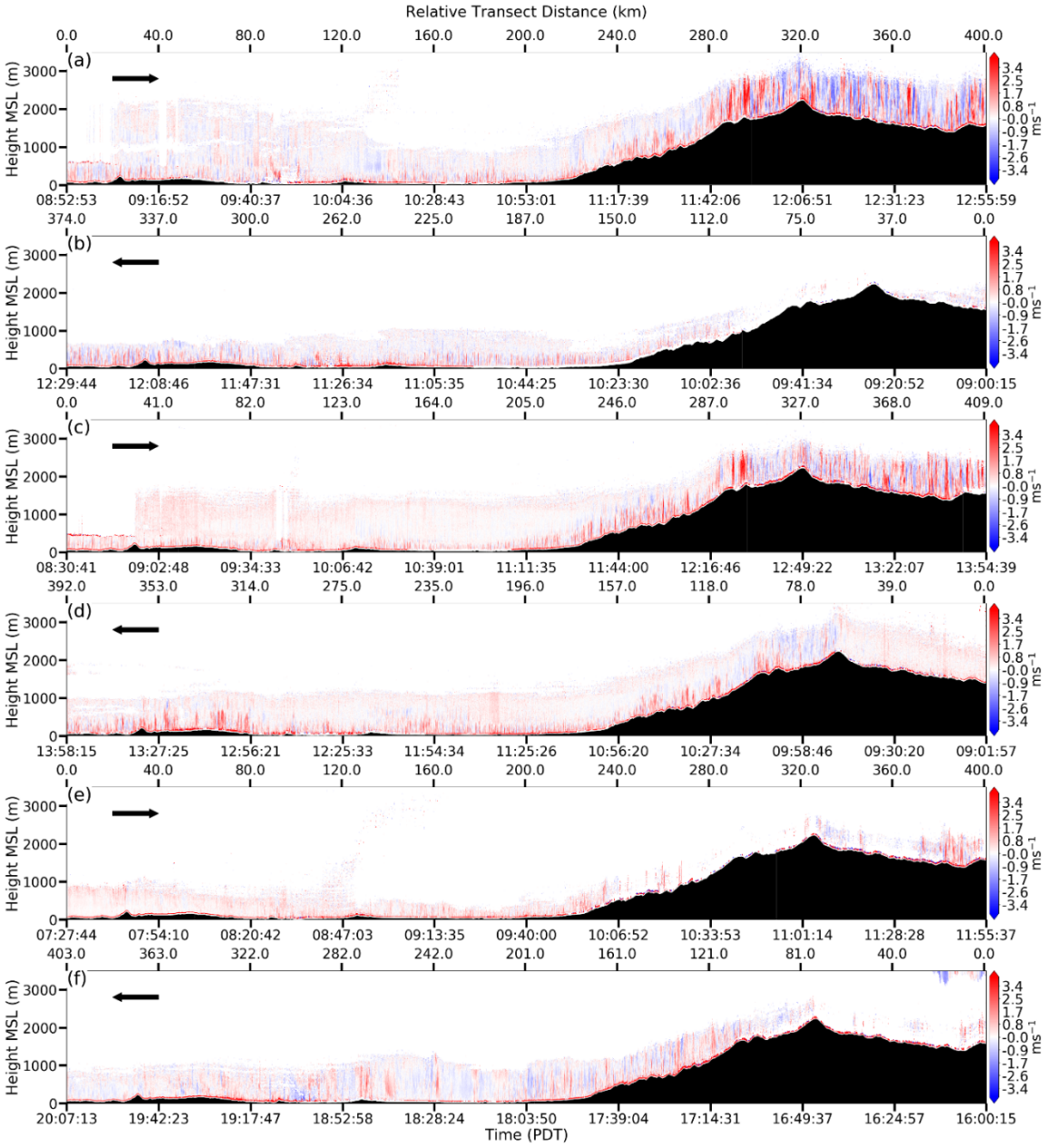

Fig. 4. As Fig. 5, but with the observed vertical velocities. The red (blue) colors denote movement away (towards) from the LiDAR

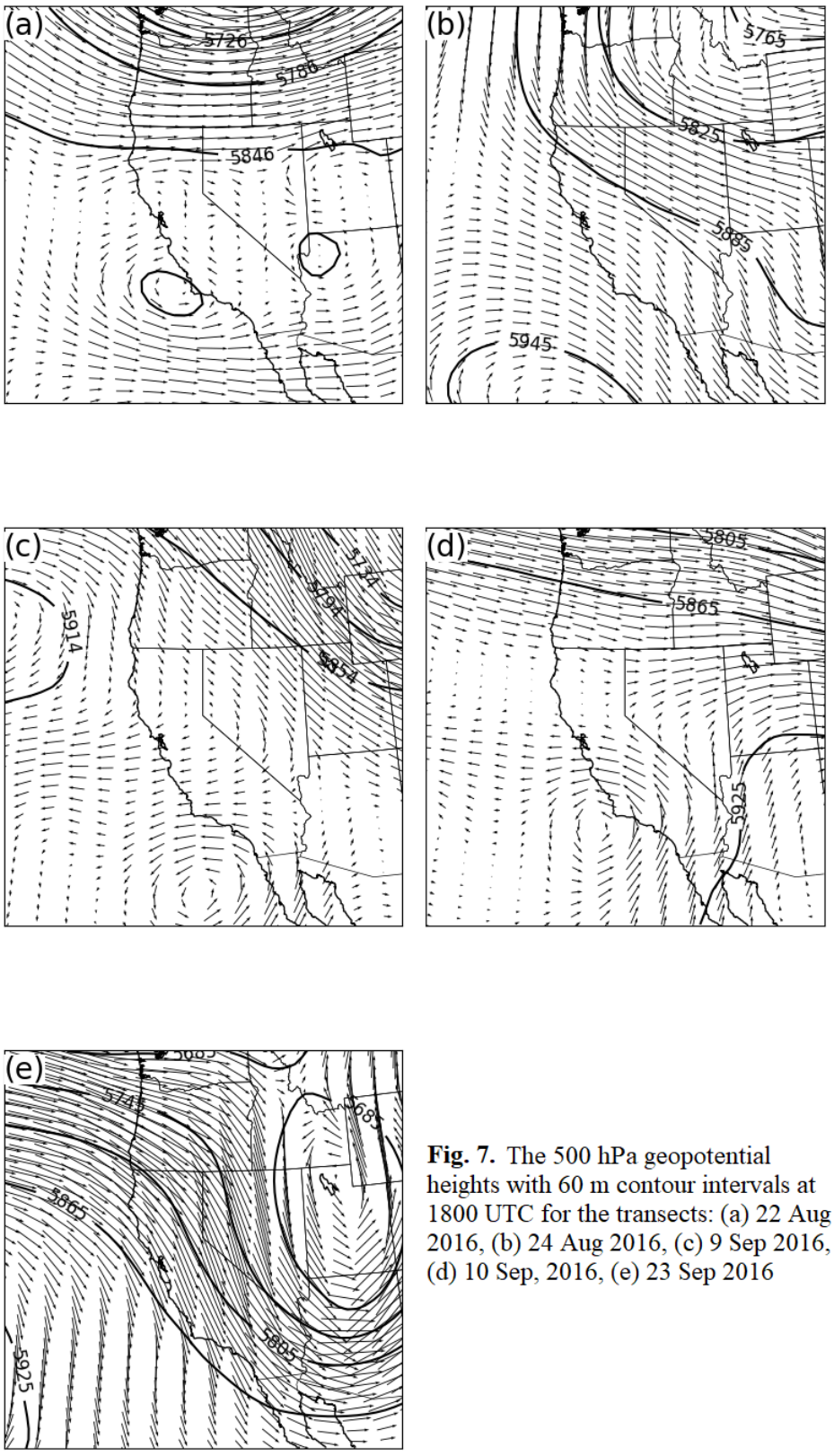

Fig. 7. The 500 hPa geopotential heights with 60 m contour intervals at 1800 UTC for the transects: (a) 22 Aug 2016, (b) 24 Aug 2016, (c) 9 Sep 2016, (d) 10 Sep, 2016, (e) 23 Sep 2016

The observed vertical velocities during the test transect on 15 June 2017 are shown in Fig. 8. The appearance of the thermals between stationary and mobile data differ. The thermals appear more narrow when mobile compared to when stationary. In addition to the differing appearance, the velocity characteristics were slightly different between the mobile and stationary sections. The average vertical velocity measured throughout all the stationary sections was 0.02 m s^{-1} with a standard deviation of 1.09 m s^{-1}. The mobile sections had an average vertical velocity of -0.08 m s^{-1} with a standard deviation of 0.98 m s^{-1}. The distribution of the data is shown in Fig. 9. The average vertical velocity profiles between the stationary and mobile sections are shown in Fig. 10. The stationary and mobile profiles show similarities, particularly with the local minima at 0.3 z/z_i. The stationary profile had a slightly positive bias compared to the mobile profile, which may be related to the velocity of CSU-MAPS during the mobile period. When accounting for CSU-MAPS velocity using equation (7), the corrected profile (solid grey line in Fig. 10) had a positive bias compared to the stationary profile. Due to the artifacts generated by this correction technique, the correction was not applied to the mobile transects.

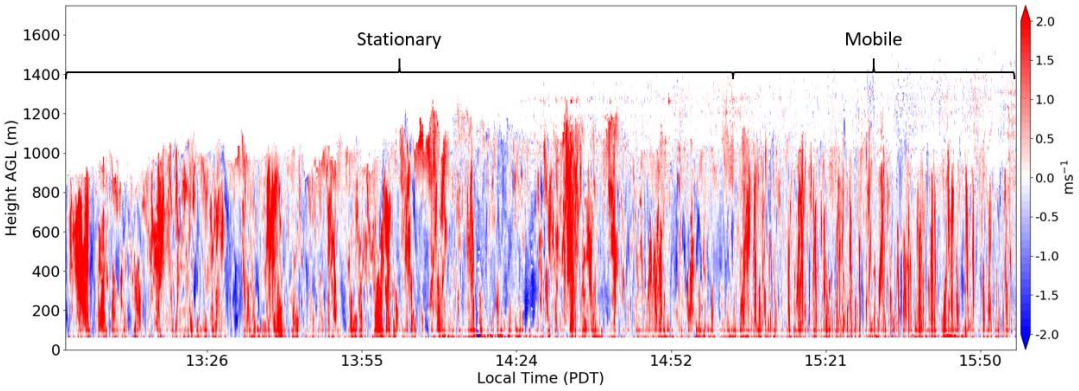

Fig. 8. The observed vertical velocities during the test transect on 15 June, 2017. CSU-MAPS was stationary from 1300-1500 PDT, and was mobile from 1500-1557 PDT.

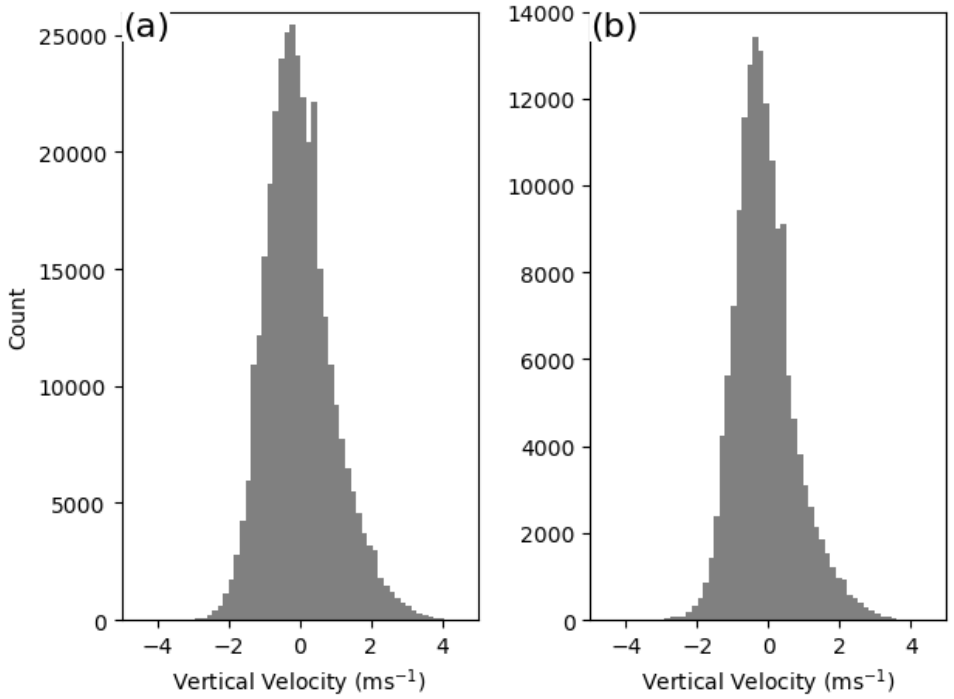

Fig. 9. Histograms of the observed vertical velocities while stationary (a) and mobile (b).

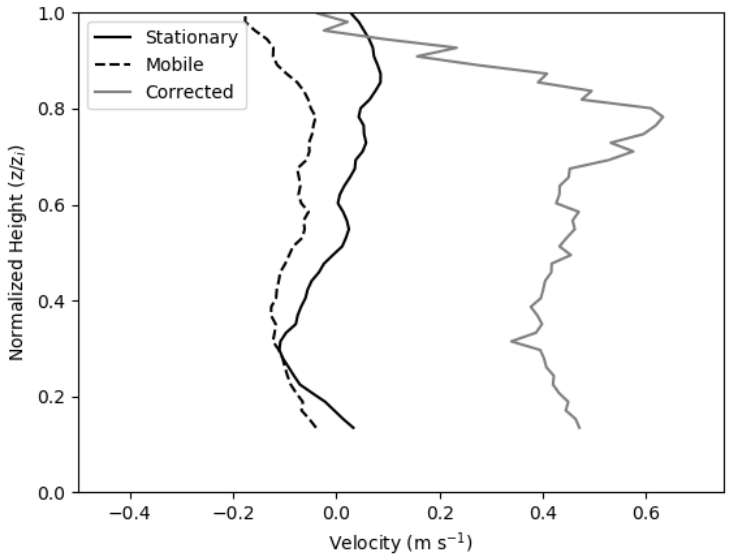

Fig. 10. Averaged profiles of the vertical velocity between the stationary and mobile periods on 15 June 2017. The solid black line is from the stationary period, and the dashed black line is the uncorrected average during the mobile period. The solid grey line is the corrected average profile during the mobile period using equation (10).

The skewness and variance profiles of the two sections also showed differences (Fig. 11). The vertical velocity variance is often normalized by the convective velocity scale (Hogan et al., 2009; Moeng and Rotunno, 1990), where the convective velocity scale (w_*) is defined as:

$$w_* = \left(\frac{g}{\overline{T_v}} \overline{w' T_v'} h \right)^{1/3}, \tag{10}$$

where g is the acceleration of gravity, T_v is the virtual temperature, $w' T_v'$ is the surface sensible heat flux, and h is the depth of the CBL.

To calculate the convective velocity scale, a sonic anemometer was deployed during the test transect and recorded the u, v, and w wind components as well as the temperature at 10 Hz. With these data and placing the top of the CBL at 1000 m AGL, w_* was calculated as 1.85 m s^{-1} during the test transect. The variance profiles (Fig 11a) showed greater variance in the stationary dataset particularly above 0.4 of the normalized CBL height (z/z_i). The stationary variance profile showed characteristics similar to the variance profile observed by Lenschow et al. (1980), with the stationary profile exhibiting a bow-like structure. Unlike the Lenschow curve, the stationary profile peaked higher in the boundary layer, around 0.6 compared to 0.4 z/z_i. The mobile variance profile did not bow as much as the stationary profile, but did peak around 0.4 z/z_i.

Under clear-sky conditions, Hogan et al. (2009) shows the skewness increases with height, and peaks at 0.6-0.8 of the normalized CBL height. Stationary and mobile profiles in the transect showed skewness increasing with height (Fig. 11b), and peaked in the same region as discussed by Hogan et al. (2009).

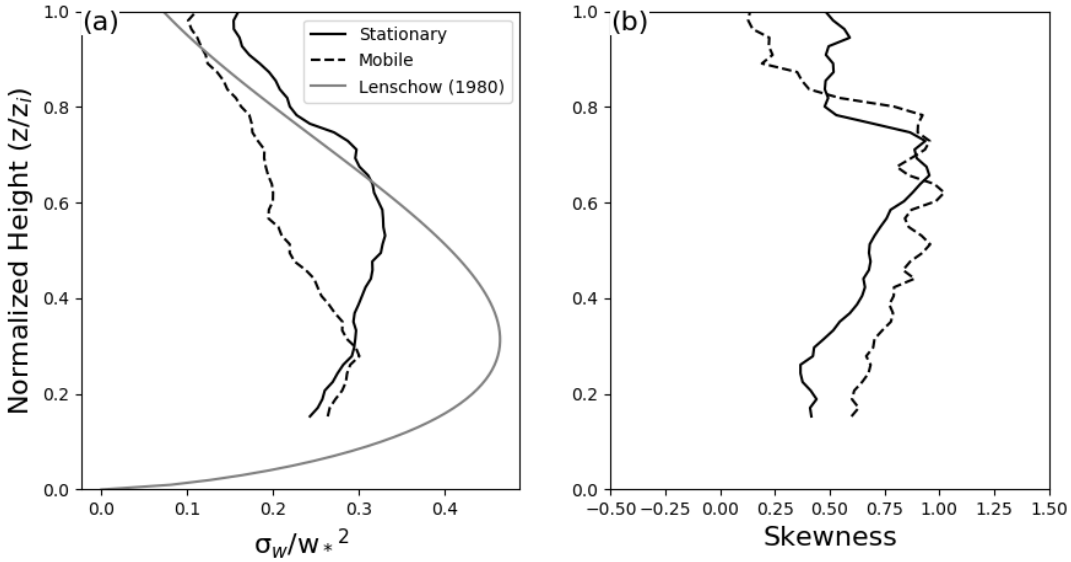

Fig. 11. Vertical profiles of the normalized velocity variance (a) and skewness (b) from the stationary and mobile data.

The mobile profile showed slightly greater skewness values compared to the stationary profile, particularly below 0.6 z/z_i. While the variance and skewness profiles between the two sections showed differences between mobile and stationary data, mobile data from this test do not show large artificial velocities in the data set. For instance, there are no anomalous spikes in the distribution that are the result of driving over bumps in the road.

b. Bay Area Transect (San Jose, CA – Vacaville, CA)

The transects on 22 Aug 2016 and 9 Sep 2016 departed San Jose during the morning, giving a morning perspective on the AL and CBL variability (Fig. 12). Marine layer stratus was present over Santa Clara Valley (0-25 km relative transect distance, hereafter RTD) during the morning hours of the two transects (Figs. 12a and 12c). The stratus was evident in the backscatter intensity profiles with full attenuation of the laser.

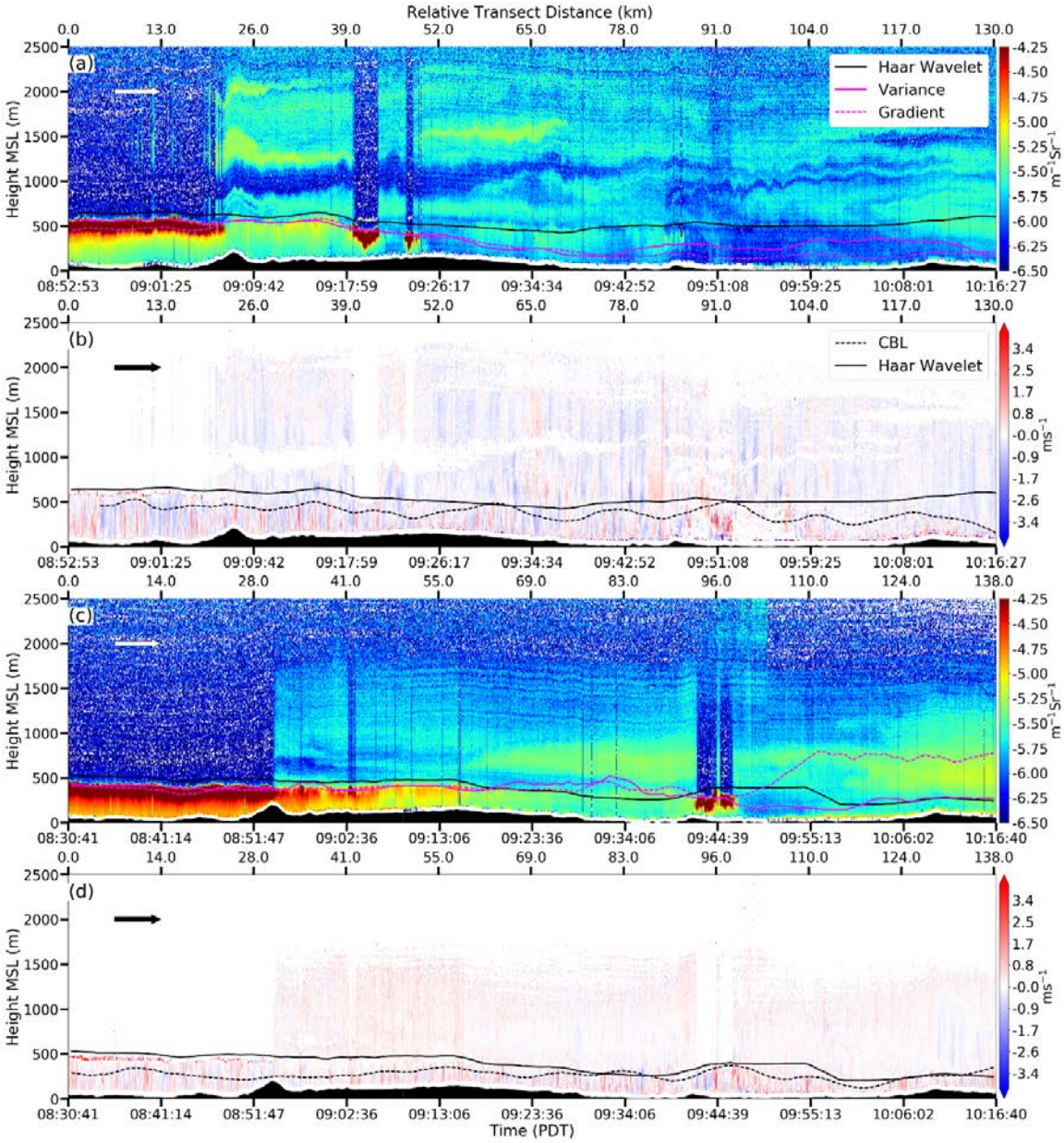

Fig. 12. Transect profiles from 22 Aug 2016 and 9 Sep 2016 along the Bay Area transect: (a) backscatter on 22 Aug, (b) vertical velocities on 22 Aug, (c) backscatter on 9 Sep, (d) vertical velocities on 9 Sep. The bottom axis displays the time associated with the transect, and the top axis displays the relative transect distance (RTD) with the arrow in the upper left indicating direction of travel. The backscatter analyses are displayed in the backscatter profiles, with the Haar wavelet analysis (solid black line) compared to vertical velocity variance analysis (dashed black line labeled as CBL) in the velocity profiles.

The stratus on 9 Sep 2016 had a cloud base height that was 100 m lower compared to 22 Aug 2016. In addition, haze was observed near the surface in the Santa Clara Valley on the morning of 9 Sep 2016. The increased backscatter intensity observed in the Santa Clara Valley was likely associated with the haze and swollen aerosols in the subcloud layer.

The vertical velocity magnitudes of updrafts within the Santa Clara Valley were more amplified on 22 Aug (Fig. 12b) compared to 9 Sep (Fig. 12d), with an average velocity of 0.75 m s^{-1} (0.58 m s^{-1}) on 22 Aug (9 Sep). The estimated CBL height by the vertical velocity variance analysis was deeper in the Santa Clara Valley on 22 Aug than on 9 Sep, but was arguably underestimated in the valley on 9 Sep compared to the observed updrafts. The 0.15 m^2 s^{-2} variance threshold lacked the proper sensitivity to the weaker vertical velocities. When the threshold was reduced to 0.08 m^2 s^{-2} (not shown), the estimated CBL was closer to what manual inspection suggests (350 m compared to 420 m, respectively). An elevated AL was also observed on both mornings, but varied in complexity and likely in origin.

The elevated AL on 22 Aug likely extended over the Santa Clara Valley, but the marine layer stratus prevented direct observations of the layer. The elevated AL was composed of multiple layers, with the bottom-most layer extending from roughly 650 – 800 m MSL. A gap of clean air 500 m in width separated the bottom portion of the elevated AL from the remainder of the elevated layer (1100 – 2200 m MSL). The source of the elevated layer was most likely smoke advected from the Soberanes fire, which was

burning south of San Jose. Visible wave structures in the backscatter (Fig. 11a) were present throughout the elevated AL, indicating the presence of gravity waves.

Visual inspection using the backscatter profiles suggested the top of the CBL outside the Santa Clara Valley was approximately 600 m MSL, where the backscatter gradient slightly drops off. The Haar wavelet analysis supported this analysis, with CBL located between 620 – 650 m MSL. In comparison, the backscatter variance derived CBL underestimated the top, placing the top around 450 – 500 m MSL at the exit of the Santa Clara Valley.

The structure of the AL within the PBL loses definition through the east bay area and into the delta (78-117 km RTD). Using the backscatter profiles, the CBL eventually becomes indiscernible due to clean air near the surface. The Haar wavelet analysis performed poorly in identifing the CBL in this clean-air region, and placed the top at the location of what is likely an elevated AL. The backscatter variance and gradient analyses suffered similar results, but placed the CBL several hundred meters lower than the Haar wavelet analysis. The CBL estimated from the vertical velocity variance was rather shallow in comparison, located around 250 m MSL. The backscatter analyses are strongly dependent on an established AL, and leads to errors in estimations of the CBL in clear-air conditions.

The overall backscatter profiles were not as complex on 9 Sep (Fig. 12c). The backscatter intensity within the elevated AL increased as CSU-MAPS approached the Central Valley. This layer was likely advected from the aerosol layer over the Central Valley, but extra analysis is required to confirm this hypothesis. All three backscatter

analyses show similar agreement outside of the Santa Clara Valley (41-85 km RTD), with the CBL placed around 400 m MSL. The three backscatter analyses showed slight disagreement in the region with cleaner air (around 0945-0956 PDT 9 Sep 2016, 96-110 km RTD). The Haar wavelet and backscatter variance analyses converged near the end of the transect, whereas the gradient analysis detected an elevated AL. The estimated CBL depth from the vertical velocity variance analysis showed similar results compared to the Haar wavelet analysis (Fig. 12d), but was more shallow on average.

Both transects showed enhanced vertical velocities while crossing over the Carquinez Strait (91 km RTD and 96 km RTD on 22 Aug and 9 Sep, respectively). This may be due to the interaction of a gap flow with the CBL, and possibly creating shear-driven turbulence. CBL depths during both transects were similar in depth after crossing the strait, averaging 228 m AGL on 22 Aug 2016 and 184 m AGL on 9 Sep 2016. On average, CBL heights on 9 Sep 2016 were 108 m lower than on 22 Aug.

The counterparts to these morning transects are the return transects from Reno - San Jose on 24 Aug and 10 Sep (Fig. 13). These transects departed Reno mid-morning and arrived in San Jose during the afternoon hours. The elevated AL observed on 22 Aug was no longer present on 24 Aug (Fig. 13a). In addition, any marine layer stratus burned off by the time CSU- MAPS sampled the Santa Clara Valley. The AL within the valley extended to approximately 600 m MSL and was a rather uniform in height. The AL was about 100 m deeper compared to the morning of 22 Aug 2016. The AL decreased in depth for a short period just beyond the edge of the valley (near Mission Pass, 98-110 km RTD), which was the result of clean air aloft penetrating the PBL. The observed vertical

velocities (Fig. 13b) showed broad downdrafts throughout the CBL in this region, accompanied with a slight decrease in the CBL height (97-111 km RTD). A well-defined updraft followed the broad downdrafts along with a rebound in the CBL depth (97 km RTD). The Haar wavelet, backscatter gradient, and variance algorithms return similar CBL tops for the majority of the transect, particularly in the Santa Clara Valley, but all deteriorated in accuracy as aerosol concentration decreased near the Carquinez Strait (42 km RTD). The Haar Wavelet placed the CBL lower than the gradient and variance analyses, and underestimated the CBL (Fig. 13a).

The transect on 10 Sep observed similar characteristics in the AL and CBL depth (Figs. 13c, 13d). The vertical extent of the AL within the Santa Clara Valley was located around 550 m AGL, an increase of roughly 100 m compared to the previous morning. In addition, the AL also temporarily decreased in depth after crossing over Mission Pass (110 km RTD).

While no broad downdrafts were observed with the decrease in the AL, the CBL depth decreased on the lee-side of the ridge (Fig. 13d to the right of Mission Pass, 110 km RTD). The similarities between the transects, which were separated by about two weeks, suggests clean air located above the marine layer is often mixed into the PBL after crossing out of the Santa Clara Valley. Flow-topography interaction over the valley ridge may be the mechanism responsible for the clean-air penetrating into the PBL. The afternoon transects also suggest a well-defined AL does not necessarily form around the Carquinez Strait.

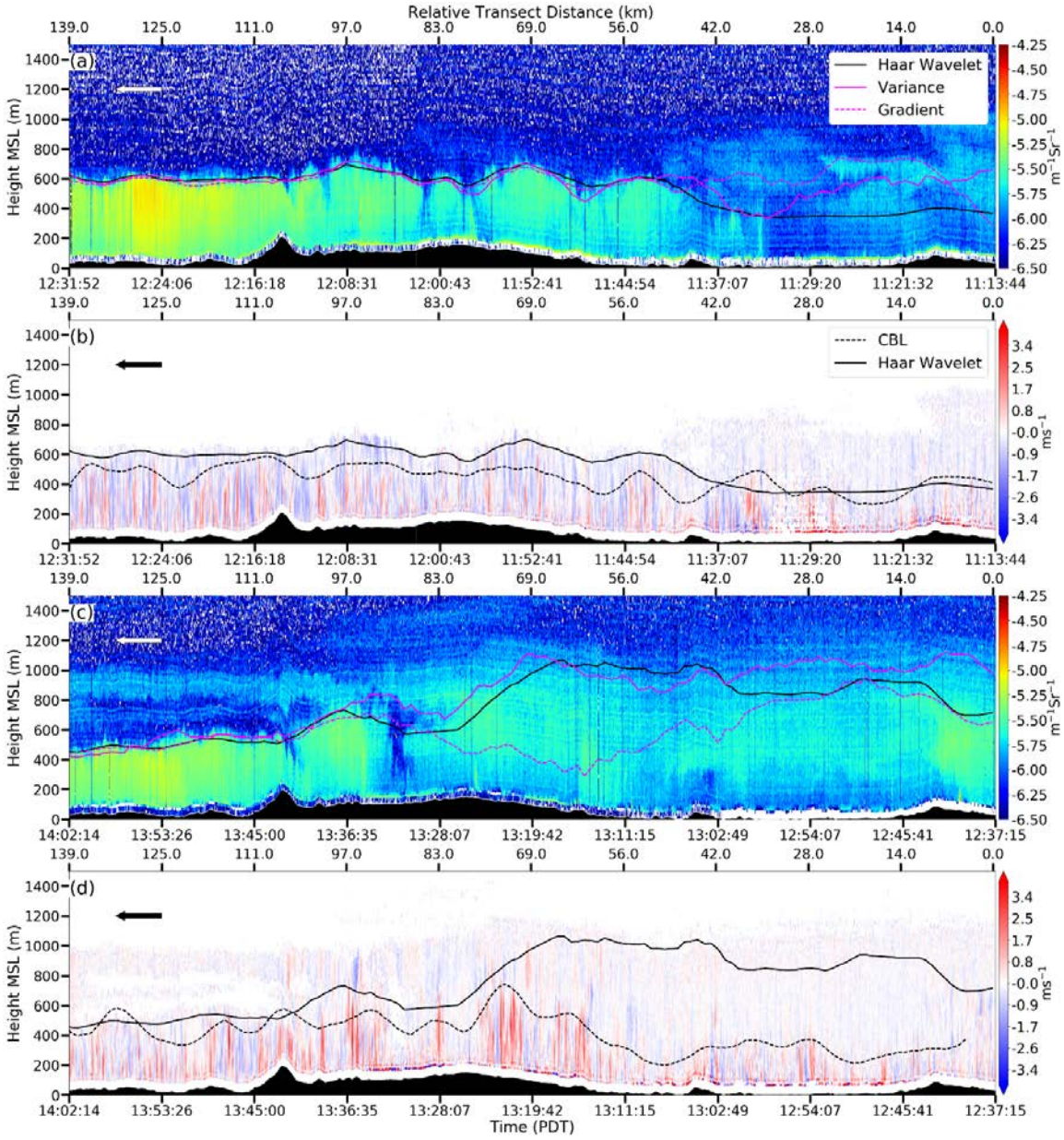

Fig. 13. As Fig. 12, but for 24 Aug 2016 and 10 Sep 2016: (a) backscatter on 24 Aug 2016, (b) vertical velocities on 24 Aug 2016, (c) backscatter on 10 Sep 2016, (d) vertical velocities on 10 Sep 2016.

While the transects on 22 Aug, 24 Aug, 9 Sep, and 10 Sep 2016 provide insight on the differing morning and afternoon AL and CBL structure, it is difficult to make direct comparisons on the temporal evolution of these variables over the course of a single day. The transects on 23 Sep (Fig 14) address this issue, as CSU-MAPS obtained a morning and evening transect profile along the Bay Area within 12 hours.

The morning transect out of San Jose on 23 Sep (Fig. 14a) differed compared to those on 22 Aug and 9 Sep. Unlike the previous morning transects, marine layer stratus was not present over the Santa Clara Valley. The AL extended to 700 m MSL in the valley, with a maximum in the backscatter returns located around 400 m MSL. Since the gradient and Haar wavelet analyses are based on detecting the location of a sharp decrease in backscatter returns, the analyses estimated the CBL just above the layer of enhanced backscatter returns. The variance algorithm performed poorly in estimating the CBL, and overestimated the depth compared to the other analyses. The level of enhanced backscatter returns extended slightly out of the Santa Clara Valley, after which the enhanced backscatter returns dissipated. The 12z Oakland sounding (not shown) indicated the marine layer capping inversion extended to 690 m MSL, roughly 200 m higher than the band of high aerosol concentrations. The capping inversion was potentially lower within the Santa Clara Valley, as suggested by the band of enhanced backscatter returns. The AL decreased in both depth and backscatter intensity through the East Bay, and was virtually non-existent shortly after passing over the Carquinez Strait (95 km RTD).

The morning transect departed San Jose around 0730 PDT 23 Sep, 1-1.5 hours earlier than the previous morning transects and only received roughly 30 minutes of incident shortwave radiation, with sunrise occurring at 0657 PDT 23 Sep. The CBL did not develop, or was too shallow to be captured by the LiDAR from 0-95 km RTD (Fig. 13b). Shallow updrafts and downdrafts were observed past 95-km RTD. These updrafts were reflected in the backscatter profile as shallow aerosol plumes (see Fig. 13a, 108 – 135 km RTD).

The backscatter profiles during the late afternoon and early evening of 23 Sep (Fig. 14c) show the depth of the AL in the Santa Clara Valley decreased by 200 m over the course of the day. Aerosol concentrations greatly diminished over downtown San Jose (138 km RTD), along with a shallower AL compared to the greater Santa Clara Valley. Similar to the afternoon profiles on 24 Aug and 10 Sep, clean air penetrating into the boundary layer was observed over Mission Pass (98 - 110 km RTD). The depth of the AL through the East Bay was shallower compared to previous afternoon transects averaging less than 300 m AGL. Close inspection of the backscatter profile over the East Bay revealed the presence of multiple stratified aerosol layers that are hyper terrain following. These returns are artifacts associated with instrument noise. While there was disagreement between the Haar wavelet, gradient, and variance in the CBL depth along the east bay, all three converged near Vacaville (0 km RTD), placing the CBL around 750 m AGL.

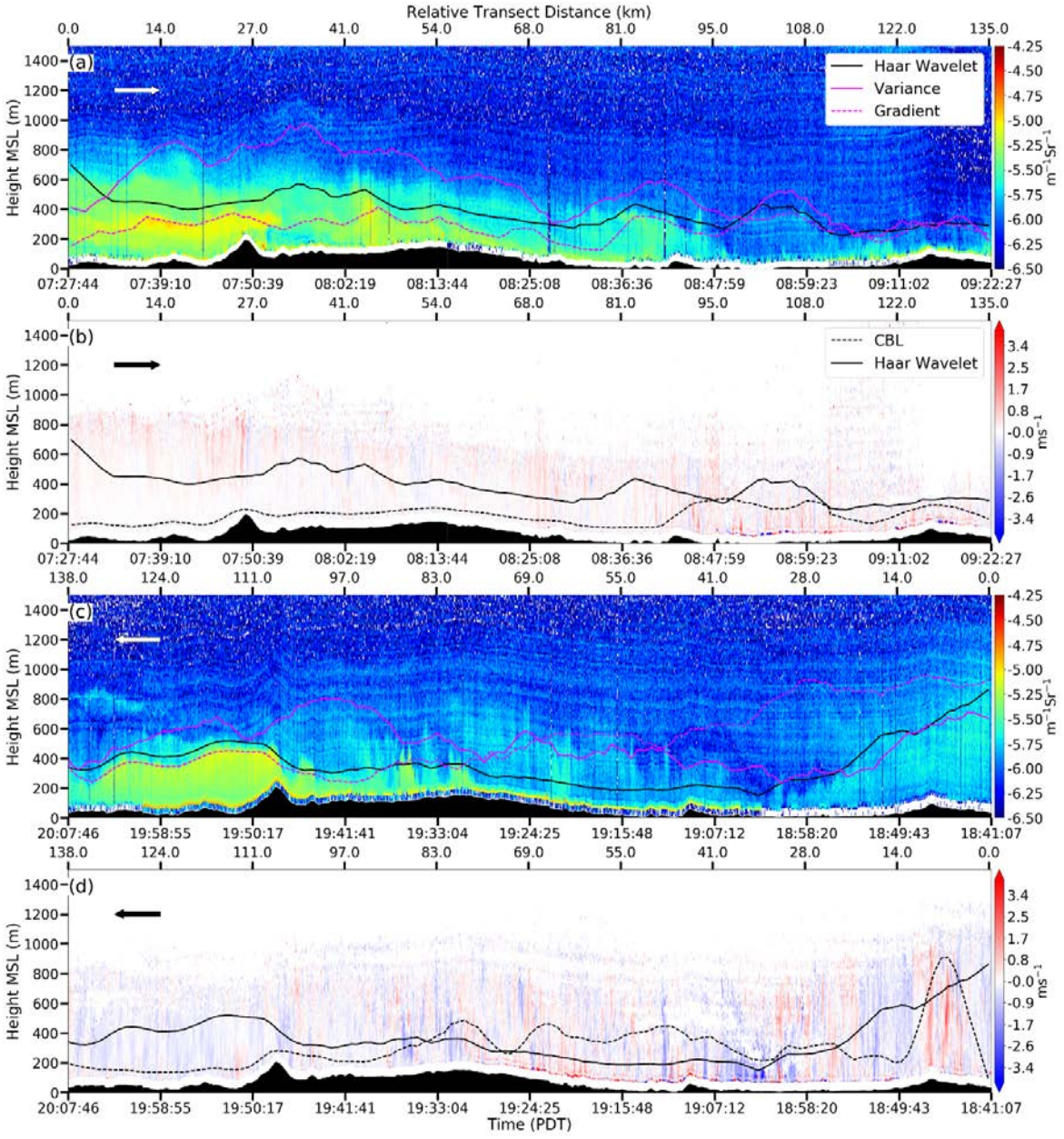

Fig. 14. As Figs. 12 & 13, but for the morning and afternoon profiles on 23 Sep 2016: (a) morning backscatter, (b) morning vertical velocities, (c) afternoon backscatter, (d) afternoon vertical velocities.

The vertical velocities within the CBL along the Bay Area transect during the afternoon of 23 Sep were not as pronounced compared to the previous afternoon transects, with mean updrafts (downdrafts) of 0.83 m s^{-1} (-0.84 m s^{-1}). The derived CBL top bulged near Vacaville (Fig. 14d), due to strong variance associated with a strong updraft core located at 600 m MSL. It is unlikely the CBL top bulged to the extent shown and is likely an overestimate. Sunset occurred at 1902 PDT 23 Sep 2016, at which point the thermal updrafts started dissipating. Updrafts largely ceased forming around 1940 PDT, leading to the cessation of the CBL development.

c. Central Valley Transect (Vacaville, CA – Roseville, CA)

The profiles along the Central Valley transect occurred at roughly the same time of day for the 22 and 24 Aug (Fig. 15) transects, as well as for the 9 and 10 Sep (Fig. 16) transects. For these transects, the central valley was sampled between 1000-1100 PDT. The transects on 23 Sep sampled the central valley at slightly different times, occurring from 0920 – 1000 PDT and from 1750 – 1840 PDT 23. Unlike the transects through the East Bay, transects through the Central Valley showed a consistent AL.

The transect on 22 Aug showed increased backscatter intensity in the PBL past Vacaville, most noticeably around 8-km RTD (Fig. 15a). The increase in backscatter instensity lead to the convergence of the three backscatter analyses around 1028 PDT (16 km RTD). The velocity variance analysis estimated the CBL around 200-m AGL, and was more accurate compared to observed updrafts than the backscatter analyses at the entrance of the Central Valley (0-8 km RTD). This was largely due to the analysis' lower estimation of the CBL near the end of the first section.

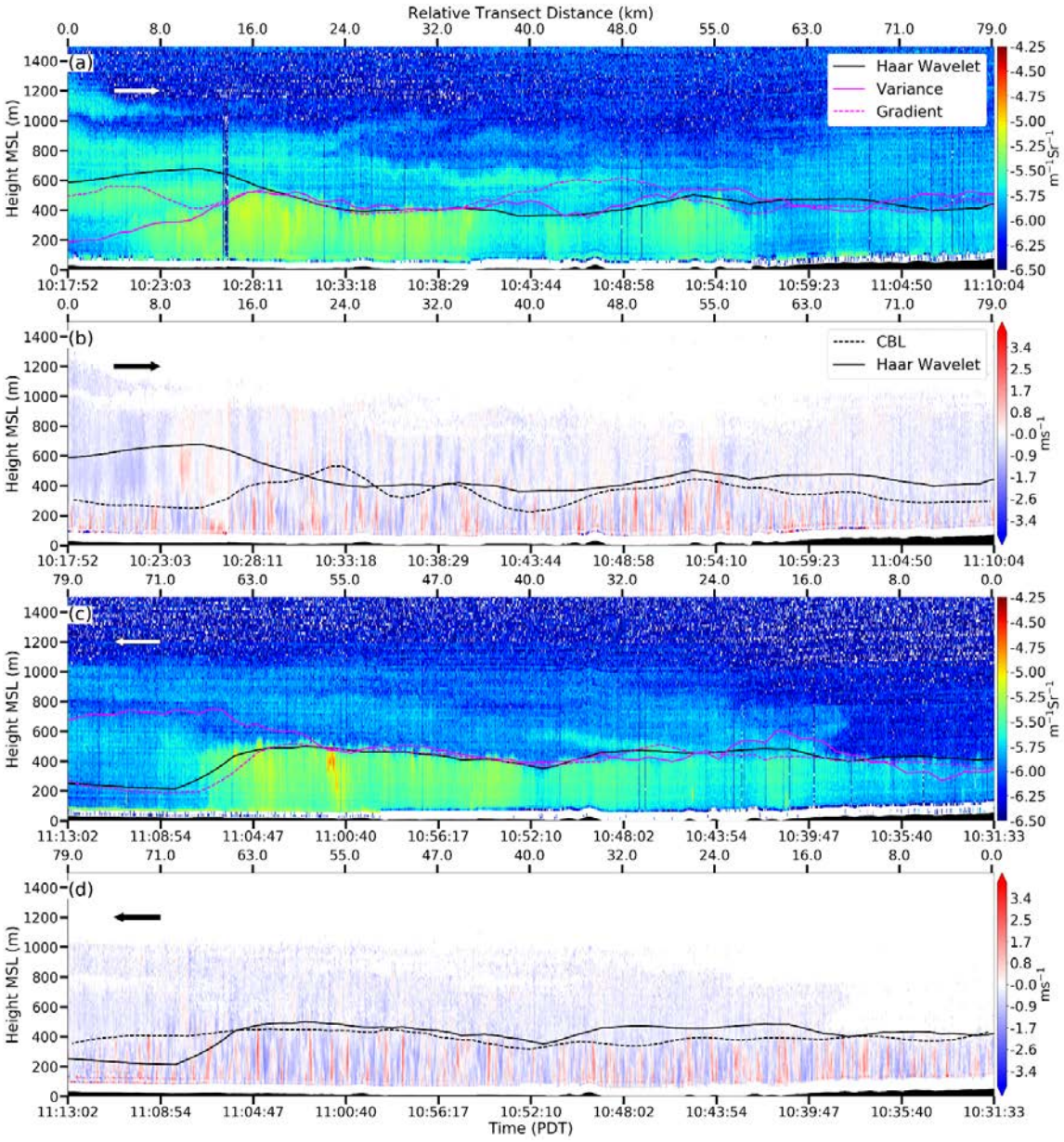

Fig. 15. Transect profiles from 22 Aug 2016 and 24 Aug 2016 along Central Valley transect: (a) backscatter on 22 Aug, (b) vertical velocities on 22 Aug 2016, (c) backscatter on 24 Aug 2016, (d) vertical velocities on 24 Aug 2016. The bottom axis displays the time associated with the transect. The top axis displays the relative transect distance (RTD), with the arrow in the upper left indicating direction of travel. The backscatter analyses are displayed in the backscatter profiles, with the Haar wavelet analysis (solid black line) compared to vertical velocity variance analysis (dashed black line labeled as CBL) in the velocity profiles.

The backscatter variance analysis initially underestimated the CBL compared to the velocity variance analysis, placing the top of the CBL 50 – 100 m lower (Fig. 15b, 0-6 km RTD). The depth of the CBL grew along with the AL, and increased to nearly 400 m AGL. The velocity variance algorithm overestimated the CBL around 24 km RTD in comparison to the observed updrafts. The overestimation was caused by the algorithm detecting gravity waves around 550 m MSL. The backscatter variance and Haar Wavelet analyses yielded similar results through the transect, and placed the CBL top around the same depth as the velocity variance analysis from 16 – 63 km RTD. The gradient algorithm returned similar estimates, but strayed from other analyses between 40-48 km RTD, as the algorithm detected an elevated AL. The average estimated depth of the CBL from the vertical velocity variance through the Central Valley was 310 m AGL, roughly 122 m lower than the estimates from the Haar wavelet (448 m AGL), variance (407 m AGL), and gradient algorithms (443 m AGL).

The profiles on 24 Aug (Figs. 15c, 15d) showed similar features to those observed on 22 Aug. Aerosol loading was minimal from Vacaville until Davis (71-79 km RTD), as denoted by low backscatter intensity returns. The backscatter analyses performed rather poorly due to the clean air, either overestimating (variance analysis) or underestimating (Haar wavelet and gradient analyses) the CBL compared to the observed thermals. Backscatter intensity returns sharply increased around 1105 PDT, allowing for a better estimation of the CBL by the backscatter analyses. The average depth of the CBL from the vertical velocity variance analysis through the Central Valley was 383 m AGL, and the average CBL between the three backscatter analyses was 420 m AGL.

A deeper AL was observed on 9 Sep, extending to 1300 m AGL (Fig. 16a). Enhanced backscatter returns were observed below 350 m AGL from 1018 -1040 PDT 9 Sep (0-40 km RTD). The variance and Haar wavelet analyses detected the layer of enhanced backscatter returns, and placed the CBL around 290 m AGL. The Haar wavelet analysis initially underestimated the CBL, but corrected itself around 1023 PDT. The variance and Haar wavelet analyses yielded similar results throughout the transect, placing the CBL within 100 m of each other on average. The two analyses diverged around 1100 PDT 9 Sep (63 km RTD), however, as the layer of enhanced backscatter returns in the CBL dissipated. The gradient analysis performed the least well out of the CBL algorithms, as the analysis overestimated the CBL by roughly 400 m over Vacaville (0-km RTD). The overestimation near the end of the East Bay transect lead to the substantial overestimation at the entrance of the Central Valley. The gradient analysis converged with the variance and Haar wavelet analyses at 1044 PDT 9 Sep (40 km RTD), after which all yielded similar results. The Haar wavelet analysis performed the most consistent out of the backscatter analyses, and yielded similar CBL depth compared to the vertical velocity variance analysis near Roseville. The vertical velocity variance analysis placed the CBL depth around 250 m AGL through the Central Valley (Fig. 16b). Closer inspection of the velocity variance derived CBL heights suggest the threshold associated with the vertical velocity variance slightly underestimated the CBL on the order of around 50 m.

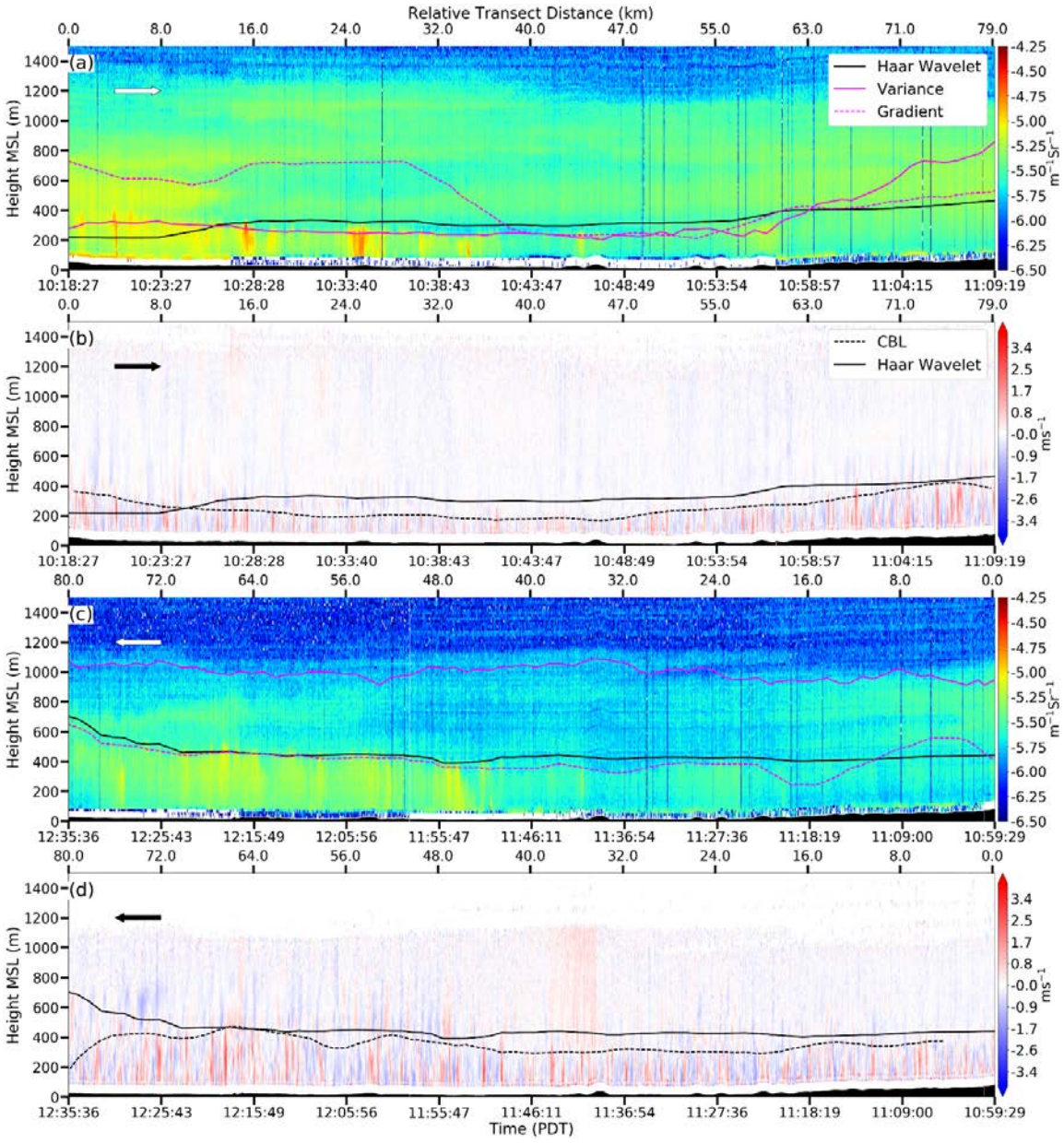

Fig. 16. As Fig. 15, but for the transects on 9 Sep 2016 and 10 Sep 2016: (a) backscatter on 9 Sep 2016, (b) vertical velocities on 9 Sep 2016, (c) backscatter on 10 Sep 2016, (d) vertical velocities on 10 Sep 2016.

The elevated AL slightly dissipated by 10 Sep, as backscatter returns weakened and the depth of the AL decreased by 150 m (Fig. 16c). Enhanced backscatter returns were observed below 500 m MSL, and were associated with the CBL (Fig. 16d). The gradient and Haar wavelet analyses placed the CBL at the top of these enhanced returns. The CBL nearly doubled in height shortly outside of Vacaville as CSU-MAPS traveled further into the Central Valley. The Haar wavelet and gradient analyses failed to capture this change in CBL depth. The backscatter variance analysis consistently overestimated the CBL during the transect, placing the CBL around 1000 m MSL. The overall depth of the CBL was similar on 9 and 10 Sep, with an average height of 250 m AGL and 350-m AGL, respectively. The velocity magnitude of the thermals on 10 Sep were slightly greater compared to 9 Sep, with an average updraft (downdraft) of 0.65 m s^{-1} (-0.61 m s^{-1}) compared to 0.58 m s^{-1} (-0.48 m s^{-1}), respectively. The deeper CBL was likely due to the difference in transect times, with the transect on 10 Sep occurring an hour later in the day.

The morning and evening transects through the central valley on 23 Sep (Fig. 17) showed substantial differences in the depth of the AL between the transects. The maximum depth of the AL in the Central Valley during the morning (Fig. 17a) extended to 500 m MSL, but decreased in depth as CSU-MAPS approached the Sierra Nevada. The backscatter intensity in the CBL also decreased near the Sierra Nevada, with the strongest backscatter returns observed between Vacaville and Sacramento (0-47 km RTD). The lower atmosphere (<1000 m MSL) was remarkably clear during the morning of 23 Sep, and was likely the result of the shortwave trough advecting any elevated

aerosol layers out of the Sacramento area.

Backscatter analyses suggested the depth of the CBL followed the that of the AL, but the derived CBL was rather shallow, particularly at the beginning of the transect (Fig. 17b). While the vertical velocity variance suggested a shallow CBL at the beginning of the transect (<200 m MSL), the CBL was slightly underestimated compared to the observed thermals between 0928 – 0936 PDT 23 Sep (8-24 km RTD). During this period, the vertical velocity variance placed the CBL around 200 m MSL, but weak updrafts extended to 350 m MSL.

The vertical velocity variance placed the CBL top at roughly the same height as the backscatter analyses at 0936 PDT 23 Sep (24 km RTD), but diverged shortly after. The vertical velocity variance also underestimated the CBL top around 0940 PDT 23 Sep (32 km RTD), with updrafts extending to nearly the same height as the backscatter analyses. To better estimate the CBL depth with weaker updrafts and downdrafts, a lower threshold value should be utilized.

The evening transect profile (occurring about 8 hours later) observed an aerosol layer 600-m deeper compared to the morning transect (Fig. 17c). The depth of the AL was not completely uniform through the transect, however, as the AL extended to 1200 m MSL over Roseville (0 km RTD). The AL depth was 400 m less over Sacramento, with the top located around 800 m MSL. The transition between the AL to the free-atmosphere over Roseville and Sacramento was associated with a sharp decline in aerosol loading. The transition grew more diffuse near Vacaville, as backscatter returns showed a gradual decrease in backscatter intensity with height.

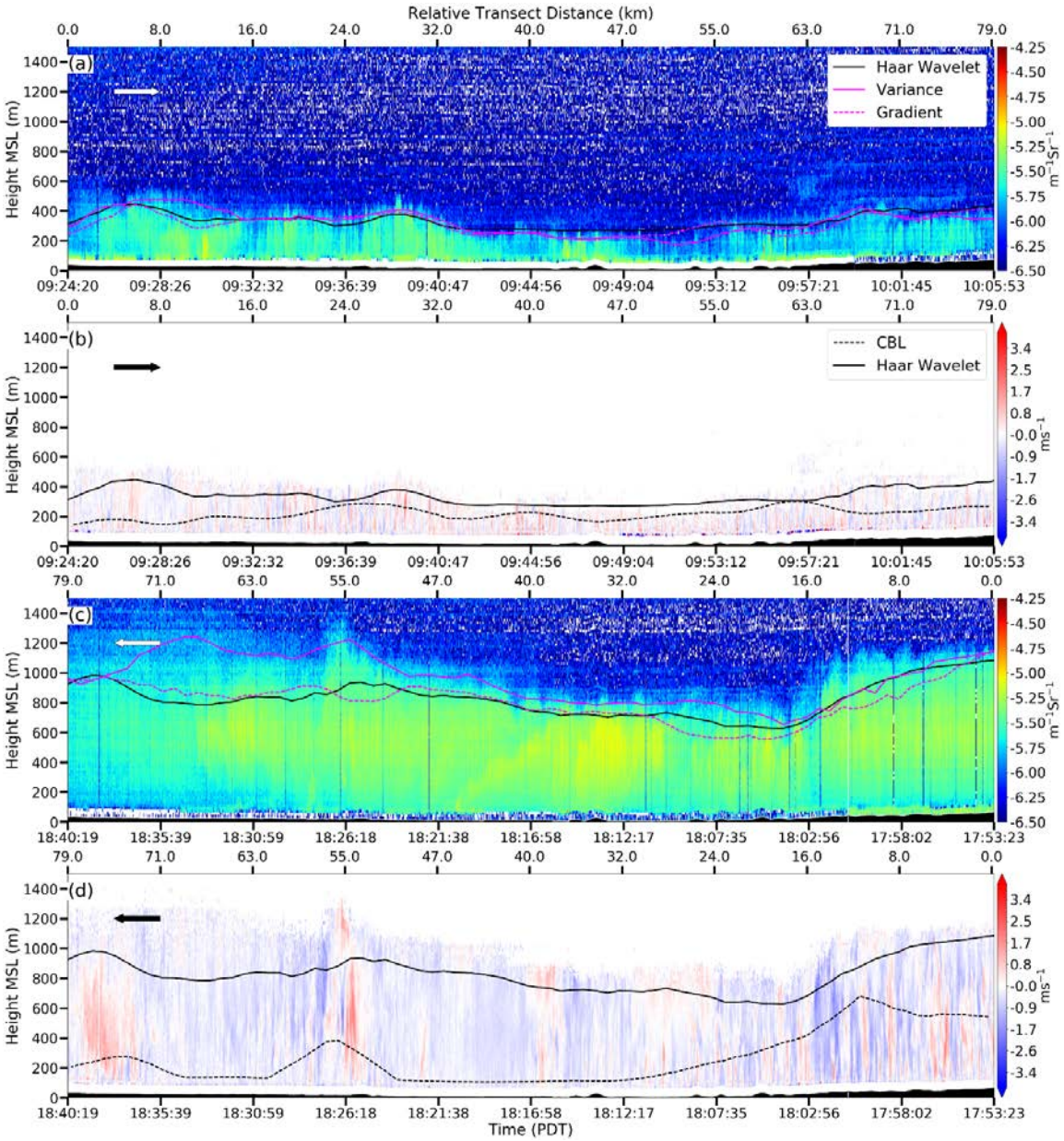

Fig. 17. As Figs. 15 & 16, but for the transects on 23 Sep: (a) morning backscatter, (b) morning vertical velocities, (c) late-afternoon backscatter, (d) late-afternoon vertical velocities.

The observed vertical velocities showed the backscatter analyses greatly overestimate the CBL for most of the evening transect (Fig. 17d). The error in backscatter analyses was least pronounced near Roseville (0-16 km RTD), as observed vertical velocities showed thermals extending to 850 – 900 m MSL. The vertical velocity variance noticeably underestimated the depth of the CBL by 300 m near Roseville. Updrafts ceased forming around 1810 PDT 23 Sep 2016, leading to cessation of CBL growth. A large updraft in terms of width and vertical extent (approximately 200 m and 800 m, respectively) was observed around 1826 PDT 23 Sep (55 km RTD). Given the time of the day and the overall size of the updraft core, the updraft was possibly driven by an atmospheric wave, a large-scale eddie that formed before the collapse of the CBL, or was generated by a sea breeze front. The updraft impacted the AL by increasing the depth of the AL by nearly 200 m compared to the surrounding region. A broader updraft with less intensity was observed near Vacaville around 1840 PDT 23 Sep (71-79 km RTD), the source of which is not as clear.

d. Sierra Nevada Transect (Roseville, CA – Reno, NV)

The presence of an AL was not always present over the Sierra Nevada during the series of cross-California transects. A visible aerosol layer was present over the Sierra Nevada on 22 Aug, 9 Sep, and 10 Sep (Fig. 18). An aerosol layer was not established over the Sierra Nevada on 24 Aug, and the weak returns prevent discussion of the structure and depth of the CBL. The AL over the Sierra tends to show similar structure between the transects. The backscatter profiles showed a layer of clean air near the surface, extending on average to 200 m AGL. The bulk of the AL lies above the clean air

layer in the mid-section, and is generally 500 – 600 m in depth. Two possible reasons are speculated for the appearance of a clean-air layer near the surface with backscatter returns above. First, the layer of clean air may be attributed to instrument noise, where the noise amplifies backscatter returns. Second, the layer of clean air may be from drainage flows advecting cleaner air from higher elevations down along the surface (McKendry et al., 1997), leaving higher aerosol loading aloft. Backscatter returns gradually tapered off above the mid-section, and the overall depth of the AL did not exceed 800 – 900-m AGL during the transects.

Aerosol loading increased with distance traveled along the western slope of the Sierra on 22 Aug (Fig. 18a). The backscatter profiles showed aerosol loading was greatest from 35-53 km RTD (1130-1140 PDT), after which backscatter returns gradually decreased towards the summit. The strongest returns in the AL extended to roughly 700 m AGL, and is represented rather well in the Haar wavelet and gradient analyses, particularly on the windward slope (0-105 km RTD).

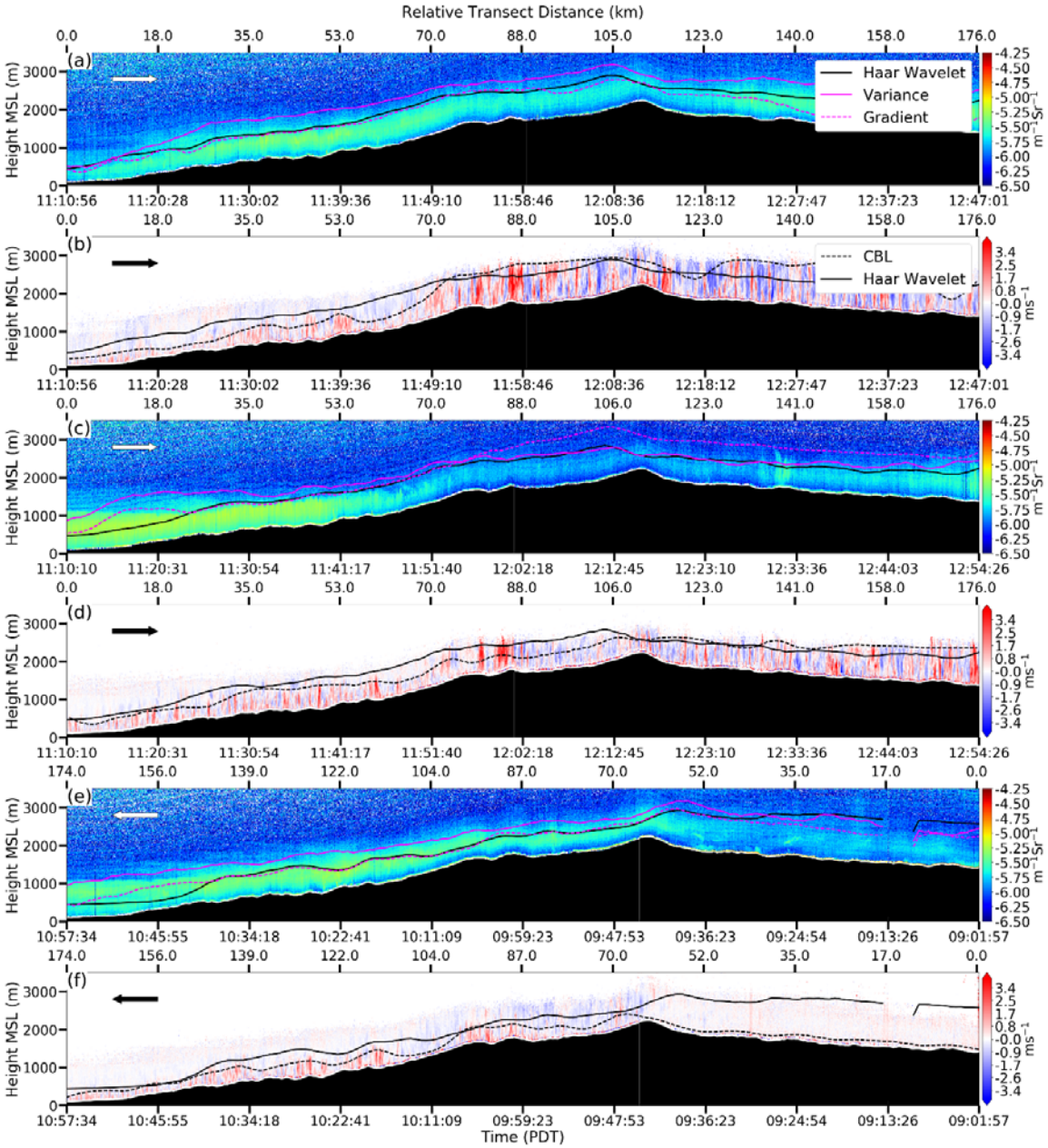

Fig. 18. The Sierra Nevada transects on 22 Aug 2016, 9 Sep 2016, and 10 Sep 2016: backscatter(a) and vertical velocities (b) on 22 Aug 2016, backscatter (c) and vertical velocities (d) on 9 Sep 2016, backscatter (e) and vertical velocities (f) on 10 Sep 2016. The bottom axis displays the time associated with the transect. The top axis displays the relative transect distance (RTD), with the arrow in the upper left indicating direction of travel. The backscatter analyses are displayed in the backscatter profiles, with the Haar wavelet analysis (solid black line) compared to vertical velocity variance analysis (dashed black line labeled as CBL) in the velocity profiles.

Comparison to the vertical velocity variance analysis showed the backscatter analyses underestimated the CBL on 22 Aug (Fig. 18b). The analyses initially performed well in the beginning portion of the transect (0-70 km RTD), as the depth of the CBL was similar to the top of the strong backscatter returns. Past 70 km RTD (1150 PDT 22 Aug), the CBL sharply increased in height as the result of enhanced vertical velocities. The Haar wavelet and gradient analyses placed the CBL at the top of the enhanced backscatter returns (located at 750 m AGL), and underestimated the CBL by 300 m.

The cause of the enhanced vertical velocities observed past 70 km RTD was most likely caused by the spatial variability of the surface sensible heat flux (Q_S). Using output from the North American Land Data Assimilation System (NLDAS), Q_S is estimated with a spatial resolution of 1/8th degree. The one hour average of Q_S showed greater sensible heat flux in the higher elevation of the Sierra Nevada compared to the Central Valley (Fig. 19). The increase in Q_S is potentially related to the presence of the coniferous forest along the west slope of the Sierra. Coniferous forests have been shown to produce greater sensible heat flux than latent heat flux, particularly above the canopy (Lee and Black, 1993). The increase in sensible heat flux most likely generated stronger thermals over the Sierra Nevada. The CBL was not uniform in depth over the Sierra, and tended to follow the overall terrain.

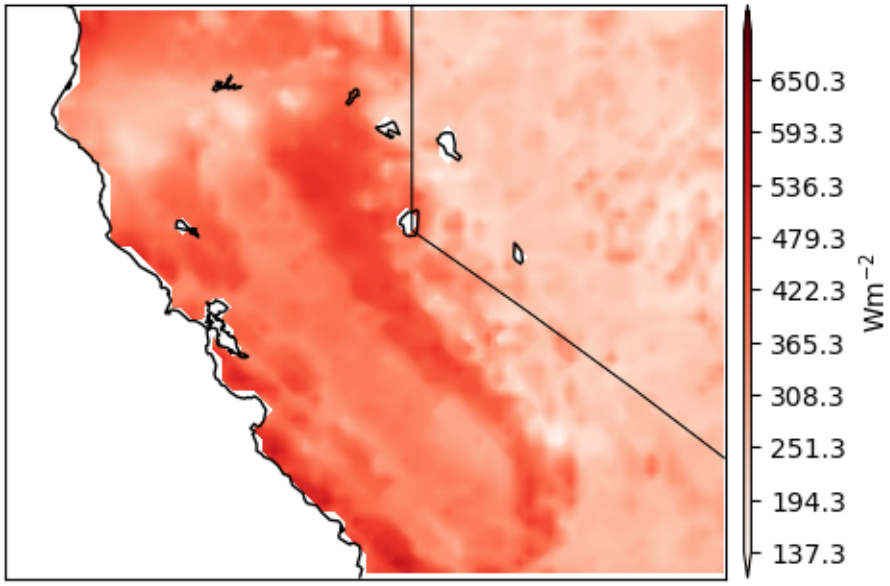

Fig. 19. The one-hour surface sensible heat flux (Q_S) output from NLDAS at 12:00 PDT on 22 Aug. NLDAS shows higher Q_S along the Sierra Nevada, and roughly corresponds with the coniferous belt.

The observed AL on 9 Sep was similar in structure to 22 Aug, but with a deeper AL over Roseville and weaker returns over the summit (Fig. 18c). Initially the AL remained nearly uniform in height over the Sierra Nevada foothills (i.e. 1110 – 1120 PDT, 0-18 km RTD). The Haar wavelet analysis overestimated the CBL by 95 m compared to the vertical velocity variance analysis over the western slope (Fig. 18d, 0-106 km RTD), but underestimated the CBL near Reno (Fig. 18d, 141-176 km RTD).

The CBL was similar in depth near Roseville on 9 Sep compared to 22 Aug, extending to 400 m AGL. Updrafts within the CBL were slightly stronger on 9 Sep, with average updrafts of 3.4 m s^{-1} compared to the average 1.2 m s^{-1} as observed on 22 Aug. Enhanced vertical velocities were observed around 1200 PDT 9 Sep, coinciding with the same region as the coniferous belt. Unlike 22 Aug, the enhanced vertical velocities were not consistently present over the summit.

The AL on 10 Sep (Fig. 18e) remained uniform in height over the foothills (156-122 km RTD) and became more terrain following 156-0 km RTD. Around 156 km RTD, the AL detrained towards the Central Valley. Light and nearly stratified backscatter returns were observed above the AL from 156-122 km RTD, and likely stems from the PBL. The detrainment may have been caused by a return circulation of the mountain-wind system, which have been observed in other mountainous regions at various times of the day (Reuten et al., 2005).

Vertical velocities within the CBL over the Sierra Nevada on 10 Sep were not as pronounced (Fig. 18f) compared to the previous transects. This was largely due to the transect occurring roughly an hour earlier in the day compared to 22 Aug and 9 Sep. Vertical velocities were nearly absent over the eastern-slope of the Sierra, along with a sharp dissipation of thermals past the summit.

The transects on 23 Sep allow for a direct comparison on the structure of the AL over the Sierra from the morning to late afternoon (Fig. 20). A direct comparison between the CBL structure was not available due to limited backscatter returns in the morning transect. The morning transect over the Sierra exhibited clean air within the PBL (Fig. 20a). Limited backscatter returns were observed over the foothills, but gradually dissipated within the first 4 km of the transect. Virtually no aerosols were detected from the foothills through the summit (18-105 km RTD). Slight backscatter returns were observed over the summit and along the eastern slope (106-175 km RTD), but did not substantially increase until CSU-MAPS arrived in Reno (175 km RTD). The Haar wavelet analysis detected very weak returns over the Sierra, placing the CBL 570 m

AGL. While the Haar Wavelet detected this weak aerosol layer, returns were too weak to provide information on the vertical velocities.

The late afternoon transect showed a stark difference in the distribution of aerosols along the Sierra Nevada (Fig. 20b). The AL over the foothills doubled in height, with backscatter returns extending to 1200 m MSL. Backscatter returns were strongest within the first 3 km of the foothills (i.e. 1753 – 1742 PDT 23 Sep, 175-70 km RTD), then gradually tapered off toward Donner Summit. The aerosol distribution indicates along-slope transport of aerosols from the Central Valley. Aerosol loading greatly decreased past the summit, with clean air observed in the PBL through Reno.

The vertical velocity variance analysis placed the CBL top slightly lower than the Haar wavelet analysis (Fig. 20c), and underestimated the vertical extent of the thermals at points along the transect, particularly in the foothills (158-175 km RTD). While neither method is perfect, the combination of the vertical velocity variance and Haar wavelet analysis provide plausible bounds on the depth of the CBL

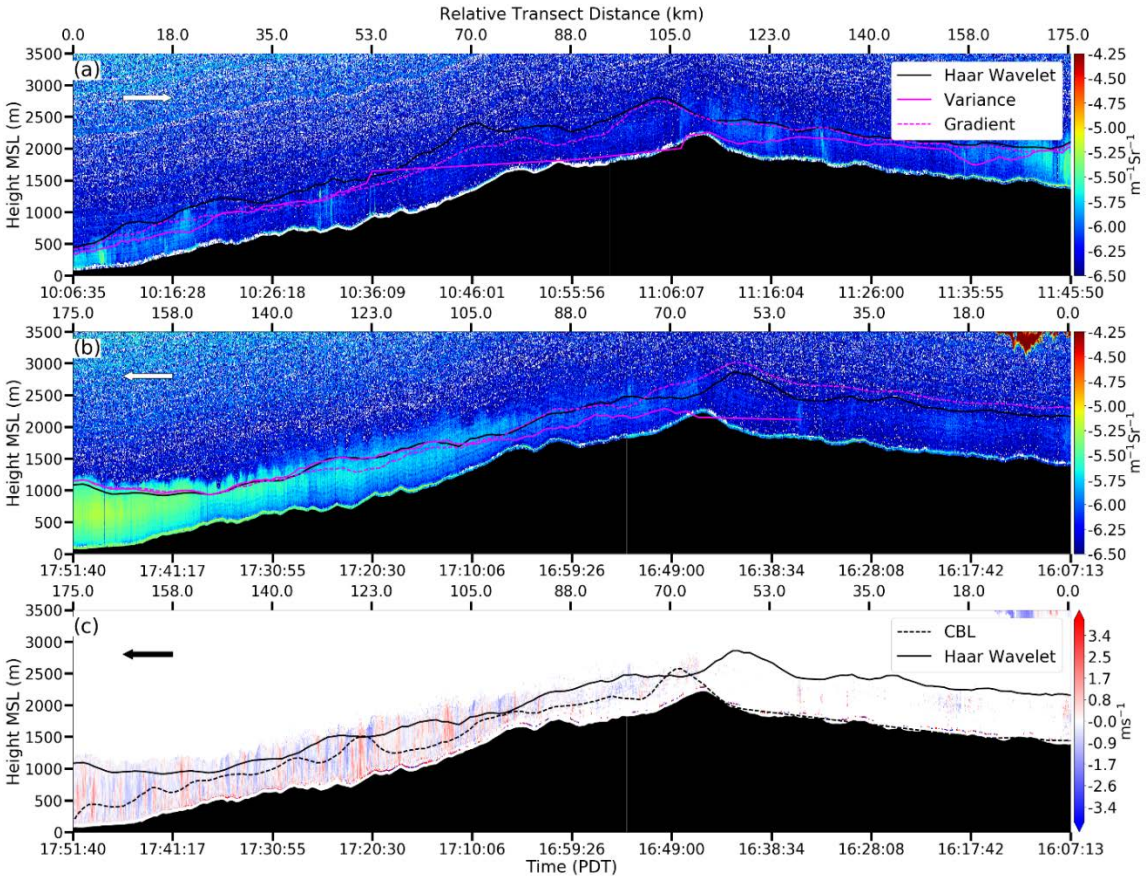

Fig. 20. As Fig. 17, but with the transects of 23 Sep: backscatter during the morning (a) and afternoon (b) on 23 Sep, and the afternoon vertical velocities (c)..

e. Variance and Skewness Profiles

Profiles of the vertical velocity variance and skewness for each section of all the transects were created for comparison (Figs. 21 and 22). The profiles were plotted against the normalized boundary layer height as calculated by the vertical velocity variance. The quality of the LiDAR returns tends to be noisy within the first 90 m, so returns were limited to those greater than 90 m in radial distance. The overall depth of the CBL is reflected in these profiles. For instance, with a shallow boundary layer (such as in the Bay Area transect on the morning of 23 Sep) the LiDAR may observe one or

two points. When these points are plotted against a normalized scale, the points will display as 0.8 -0.9 of the normalized height. This is the reason why various skewness and variance profiles do not fully extend down towards the surface, and are limited above 0.5 the normalized height.

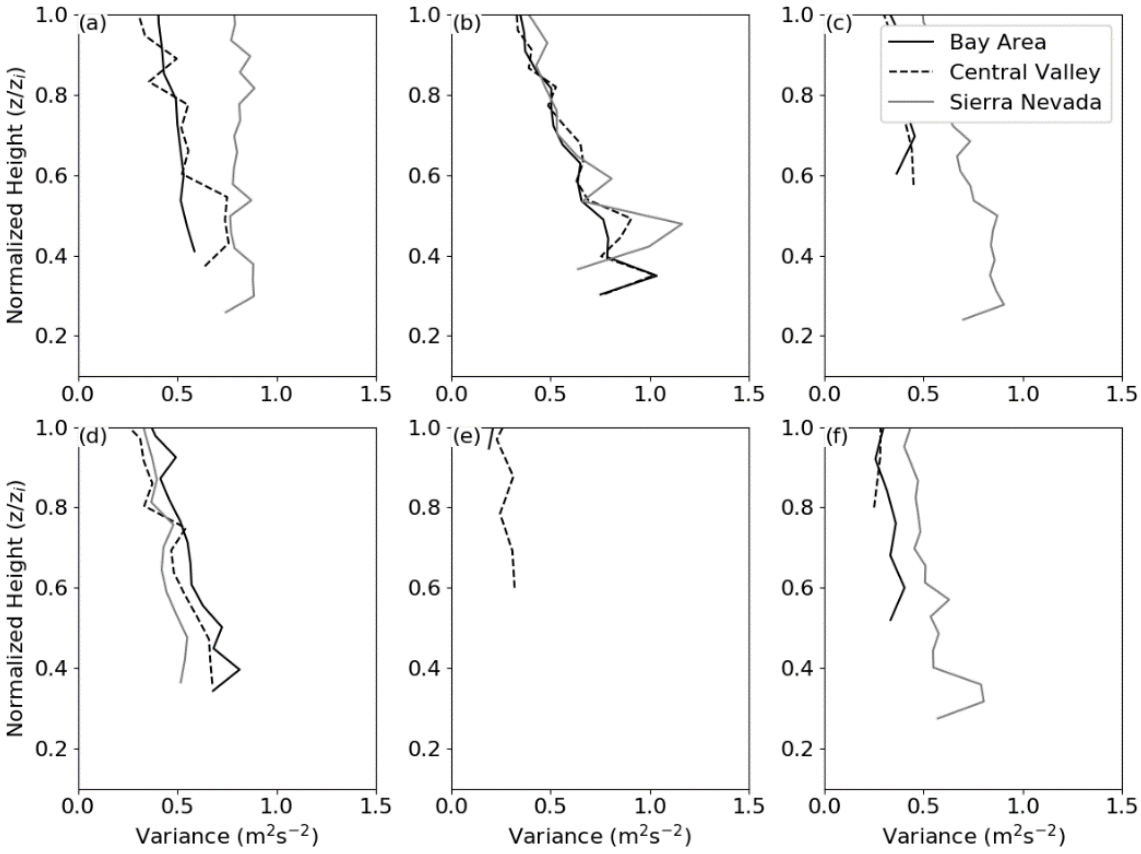

Fig. 21. The average variance profiles of the three sections from each transect: (a) 22 Aug 2016, (b) 24 Aug 2016, (c) 9 Sep 2016, (d) 10 Sep 2016, (e) morning of 23 Sep 2016, (f) afternoon of 23 Sep 2016. These profiles are plotted against the normalized height from the estimated CBL depth (z/z_i). A shallow CBL results in a profile that does not extend down far past 1.0 z/z_i, such as the profiles observed in (e).

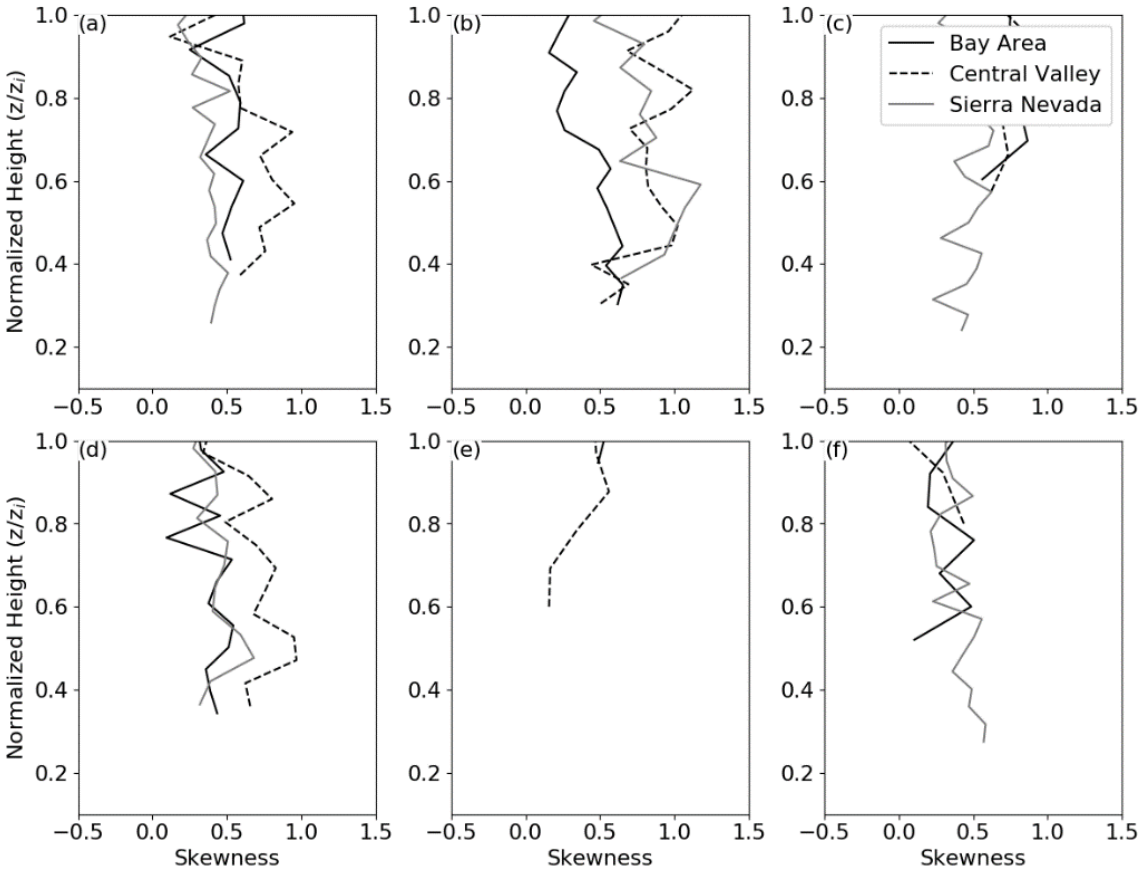

Fig. 22. As Fig. 21, but with average skewness profiles.

With these profiles, composite variance and skewness profiles of the three sections across multiple transects were created (Fig. 23). When creating the composite, transects with shallow boundary layers were omitted, such as transects on 9 Sep and 23 Sep. The composite profiles were constructed using the 22 Aug, 24 Aug, and 10 Sep transects. The composite variance profiles show similar structure between the three sections, with variance decreasing in height (Fig. 23a). Typical variance profiles of the CBL, when stationary, show a bow-like profile with the highest variance near the middle of the CBL (Hogan et al., 2009). Weissmann et al. (2005) analyzed the vertical velocity variance from an airborne Doppler LiDAR, and showed a variance profile similar to the composite

profile, but with slightly lower variance. The smaller variance may be the result of the coarser spatial resolution of the data, the smaller range of observed vertical velocities, or different buoyancy forcing at the surface.

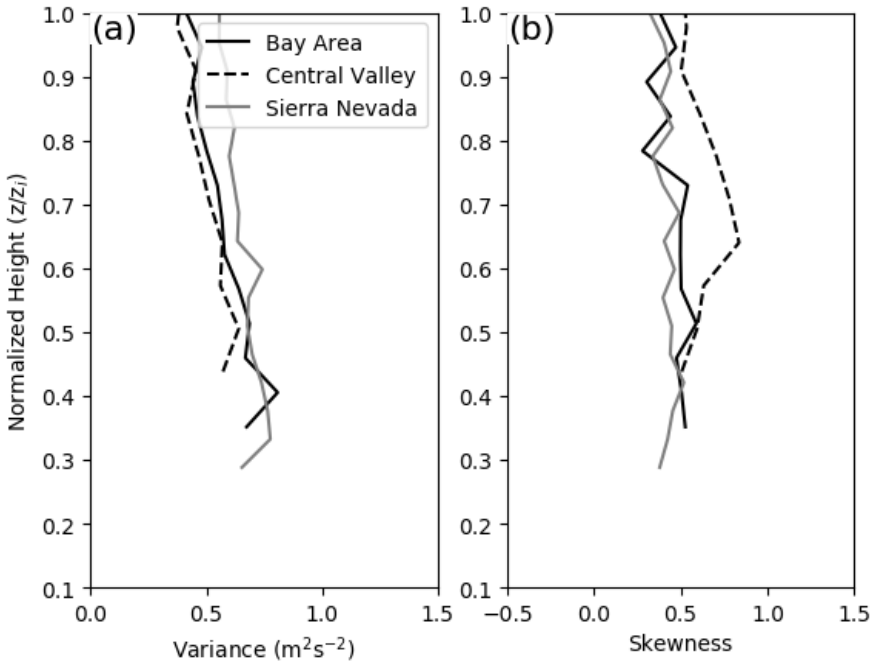

Fig. 23. Composite variance and skewness profiles of all three sections from transects with established CBLs (e.g. 22 Aug 2016, 24 Aug 2016, 10 Sep 2016). Similar to Figs. 20 and 21, the profiles are plotted against the normalized CBL height (z/z_i).

The composite skewness profiles were slightly different in structure between the three sections (Fig. 23b). The skewness profiles of the Bay Area and Sierra Nevada transect were similar, with both profiles centering around 0.45 throughout the CBL. The Central Valley transect composite profile showed more variability with height in the CBL, with skewness values peaking at 0.65 of the normalized CBL height. The composite is similar to skewness profiles under clear-sky conditions, with skewness increasing with height (Moyer and Young, 1991; Hogan et al. 2009). The more standard skewness profile associated with the Central Valley transect is arguably a sign the turbulence within the

CBL was predominantly generated through surface heating. While surface heating is a primary source of turbulence in the Bay Area and Sierra Nevada transects, turbulence is also likely influenced by the marine layer (local wind circulations) in the California Bay Area (Sierra Nevada). Analysis of mobile observations on skewness is limited in the literature, making comparisons of these data to other studies difficult.

f. Soberanes Fire Transect

The Soberanes fire was one of the largest incidents in California's 2016 wildfire season, burning 53,470 hectares in total. The fire was ignited on 22 Jul 2016 in the Santa Lucia mountain range, 12 km south of Monterey, CA. CSU-MAPS sampled the fire on 26 Jul 2016 (Fig. 24) and the incident grew slightly over 2,300 hectares over the course of the day.

A closed high located over the Nevada and Arizona border generated south-easterly flow along the Californian Coast (Fig. 25a). The south-easterly flow diverged near the Bay Area, with the 500 hPa winds transitioning to more easterly over the ocean, and more westerly inland. As a result, much of the smoke emitted from the Soberanes fire was transported inland and over the Bay Area.

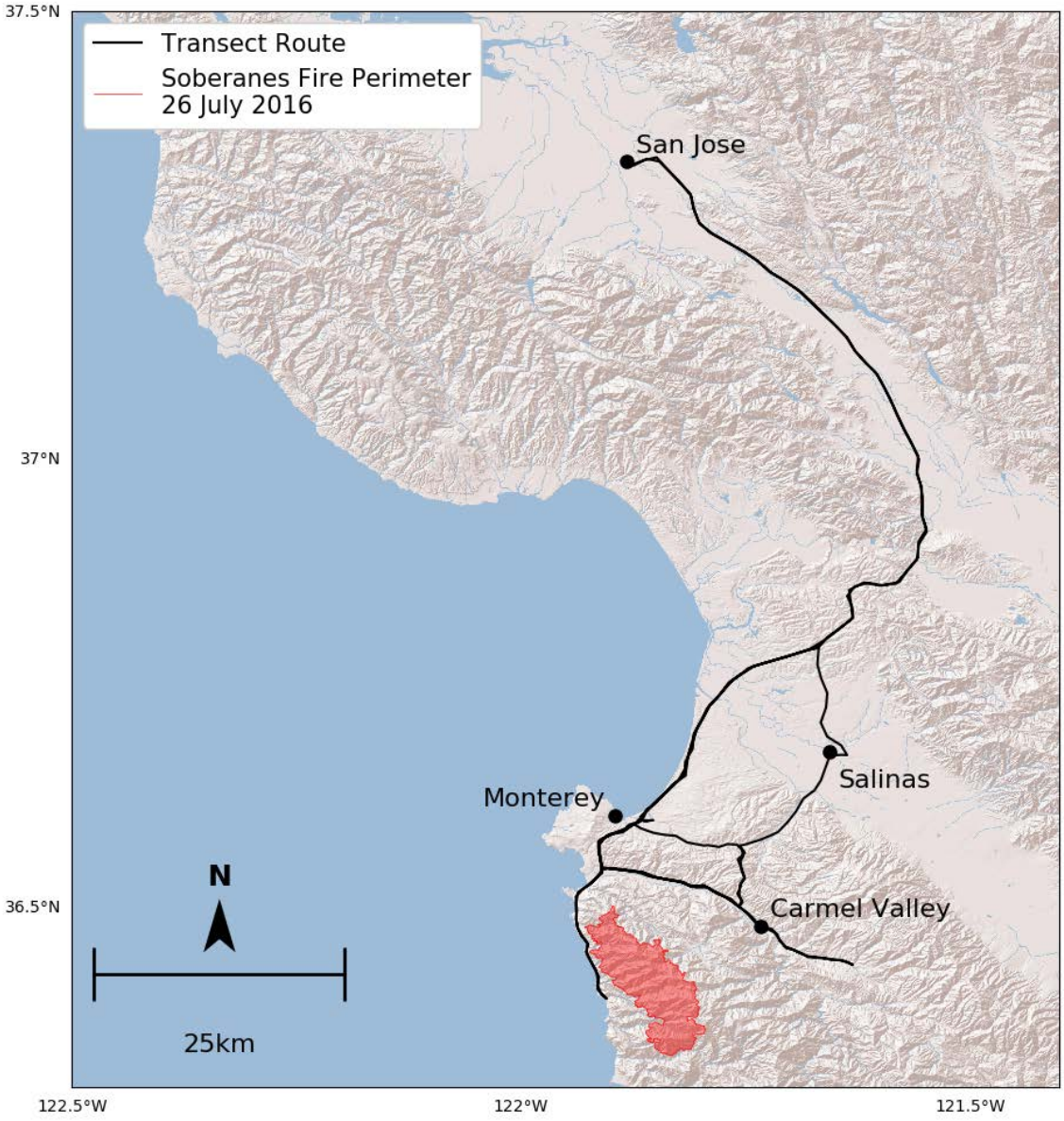

Fig. 24. Map of the Soberanes fire perimeter and the transect route

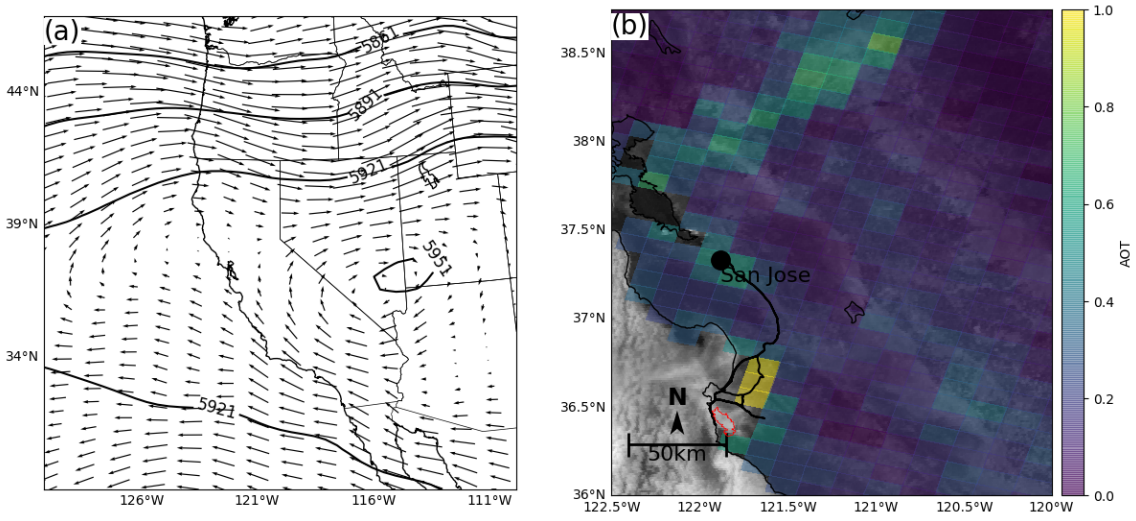

Fig. 25. Synoptic conditions on 26 July 2016. The 500-hPa geopotential heights (a) show anti-cyclonic circulation over the California, Nevada, and Arizona borders. The south-easterly winds associated with the circulation advected smoke from the Soberanes fire North, which is reflected in the MODIS AOT retrievals (b).

The Moderate Resolution Imaging Spectroradiometer (MODIS) onboard the Terra polar-orbiting satellite, passed over the Soberanes fire at 1220 PDT 26 July 2016. MODIS provides estimates on the AOT over land in 3 km swaths. The corrected AOT over land showed high AOT over the Salinas Valley, with an AOT close to 1 (Fig. 25b). AOT retrievals were unavailable over the immediate area of the fire, as the AOT retrieval algorithm likely misidentified the smoke plume as a cloud. AOT retrievals showed smoke from the Soberanes fire extending from the Bay Area through the Central Valley, with values around 0.5 were observed in the Santa Clara Valley. The greater optical thickness in the Santa Clara Valley compared to the surrounding region is likely due to the combination of an elevated smoke layer, and typical aerosol loading in the valley.

The Soberanes transect was separated into three sections: (1) the Santa Clara Valley, (2) the Salinas Valley, and (3) the Carmel Valley. Within these sections, the vertical velocity variance and Haar wavelet analyses were used to estimate the CBL depth.

Results from the cross-California suggest the Haar wavelet analysis generally outperforms the gradient and variance analyses, so the two analyses were omitted from the Soberanes transects.

g. Santa Clara Valley

CSU-MAPS departed San Jose and drove south through the Santa Clara Valley between 1030 – 1112 PDT 26 July 2016. Backscatter profiles (Fig. 26a) showed the AL extending to 500 m MSL, with an elevated smoke layer extending from 750 – 1900 m MSL (hereafter primary smoke layer). Another elevated smoke layer was observed near 2500 m MSL, but was much smaller in depth compared to the primary smoke layer. The clean air gap between the primary smoke layer and the AL decreased as CSU-MAPS traveled south in the valley, with the gap disappearing around 1047 PDT 26 July 2016. In general, the strongest backscatter returns occurred within the primary smoke layer and not within the AL, as was observed in the previous transects through the Santa Clara Valley.

While the primary smoke layer changed the surface energy budget (e.g. Robock, 1988; Wang and Christopher, 2006), the smoke layer was not optically thick enough to fully suppress the development of the CBL. The vertical velocity variance through the Santa Clara estimated the CBL at 200 m AGL on average, with the Harr wavelet analysis estimating the CBL slightly higher at 377 m AGL (Fig. 26b). The average updraft and downdraft velocities in the CBL were nearly equivalent, with velocities of +0.44 and -0.44 m s^{-1}. The CBL depth within the Santa Clara Valley was slightly more shallow compared to the morning transects on 22 Aug and 9 Sep 2016. The average depth of the

CBL during these transects was 220 m AGL, ~20 m deeper than on 26 July 2016. Further investigation is needed to adequately determine the full influence of the smoke layer on the surface energy budget, and in-turn on CBL growth.

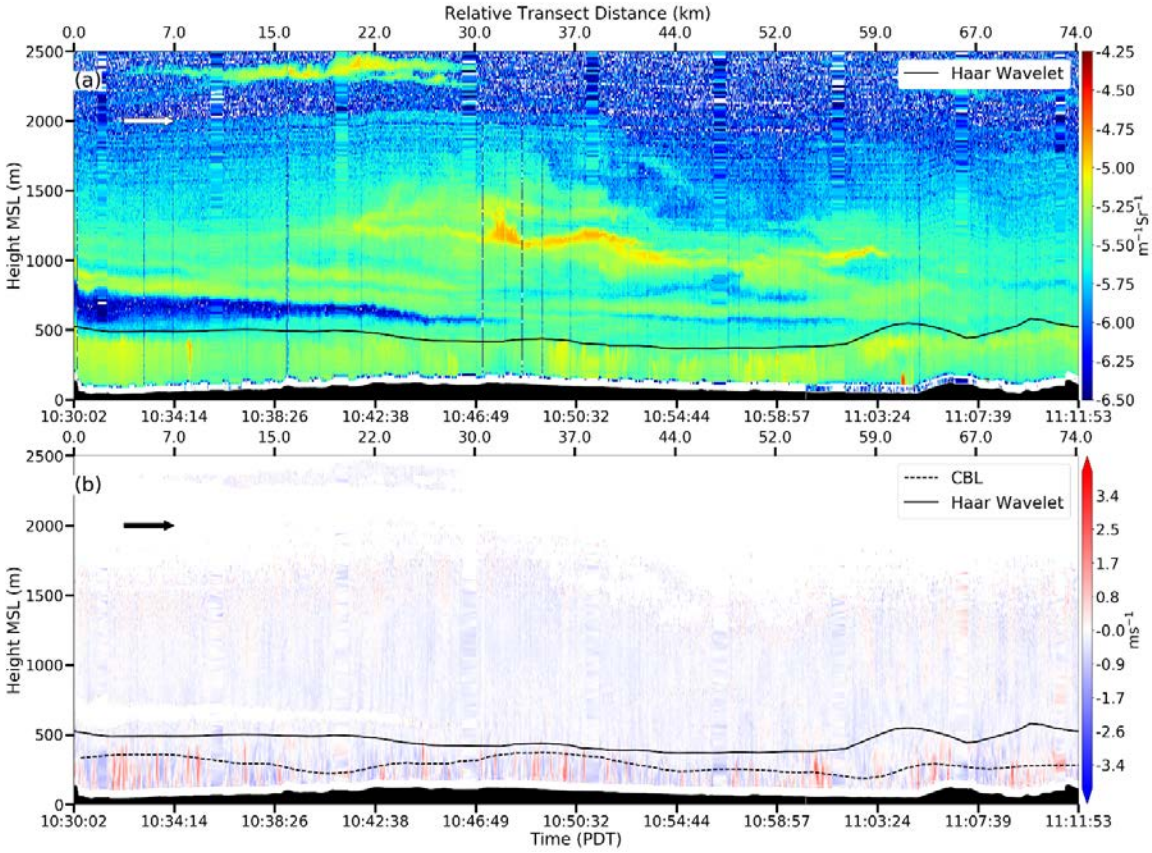

Fig. 26. The backscatter (a) and vertical velocity (b) profiles through the Santa Clara Valley on 26 July. The bottom axis displays the time associated with the transect. The top axis displays the relative transect distance (RTD), with the arrow in the upper left indicating direction of travel. The backscatter analyses are displayed in the backscatter profiles, with the Haar wavelet analysis (solid black line) compared to vertical velocity variance analysis (dashed black line labeled as CBL) in the velocity profiles.

h. Salinas Valley

The structure of the smoke layer was more complex within the Salinas Valley compared to the Santa Clara Valley (Fig. 27a). The heaviest aerosol loading was observed near the surface, below 500 m MSL. Traces of smoke above the strong returns extended to 1500 m MSL. Two elevated smoke layers were also observed at 2250 m MSL and 2750 m MSL, each around 150 m thick. CSU-MAPS drove out from under the elevated layer at 2750 m MSL roughly halfway through the transect, whereas the other layer was present throughout and increased in both thickness and backscatter intensity near the end of the Salinas Valley.

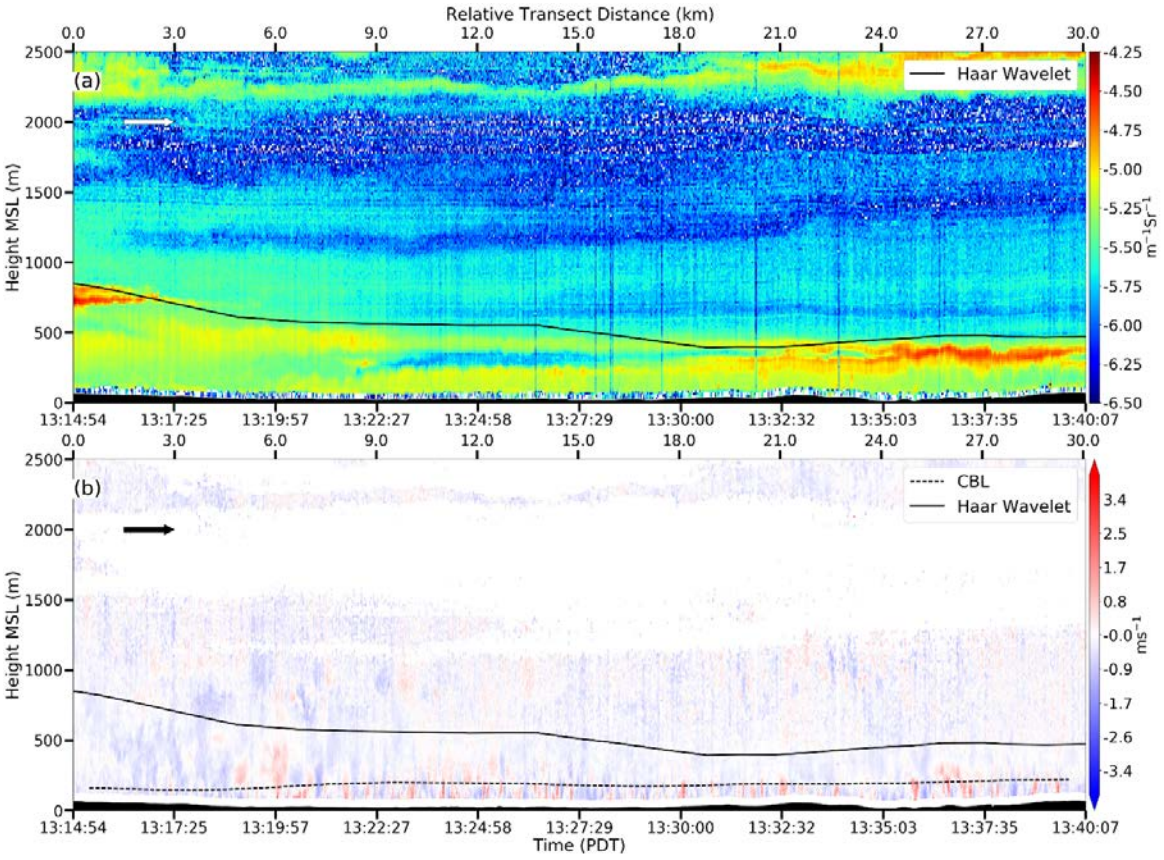

Fig. 27. As Fig. 25, but for the backscatter (a) and vertical velocity (b) profiles through the Salinas Valley.

Closer inspection of the backscatter profiles between 1314 - 1318 PDT revealed a layer of stronger backscatter returns located at 500 m MSL. At 1320 PDT (6 km RTD), another layer of strong backscatter returns started forming near the surface, below 250 m MSL. The formation of these backscatter returns suggests the profiles are associated with the CBL. A layer of clean air was observed around 250 m MSL between 9 - 15 km RTD, further suggesting the presence of a shallow CBL.

Observed vertical velocities in the Salinas Valley were rather weak, particularly within the smoke layer (Fig. 27b). A broad region of vertical motion was observed between 1315 – 1317 PDT, extending to 500 m MSL. The Haar wavelet analysis placed the CBL at the same height as the vertical extent of the broad updraft. This broad updraft did not exhibit characteristics to previously observed thermals in terms of updraft width and strength. The broad region of updrafts was likely not solely driven by surface based convection, and was influenced by another mechanism. Thermals associated with the CBL developed around 1318 PDT, and extended 152 m AGL on average. The growth of the CBL was likely limited by the optically thick smoke layer. Although it is difficult to compare to boundary layer heights in the Salinas Valley to the Santa Clara Valley due to the spatial separation, CBL heights were 50 m shallower in the Salinas Valley. While the CBL was more shallow, the vertical velocities within the CBL were slightly greater, averaging around 0.63 m s^{-1} for updrafts and 0.55 m s^{-1} for downdrafts, 0.19 m s^{-1} (0.11 m s^{-1}) stronger than the updrafts (downdrafts) in the Santa Clara Valley. The stronger updrafts (downdrafts) are expected, however, primarily due to the difference in timing of the transects (i.e. mid-morning compared to mid-afternoon).

i. Carmel Valley

The transect through the Carmel Valley occurred later in the afternoon, from 1454 – 1523 PDT 26 July 2016. The greatest aerosol loading throughout the Soberanes transect was observed in the Carmel Valley (Fig. 28a). In addition to the greater aerosol loading, the backscatter profiles were the most complex in the Carmel Valley. The backscatter profiles also confirm the speculation that the MODIS AOT retrieval algorithm misidentified the smoke plume as a cloud layer, which prevented an estimation on the AOT.

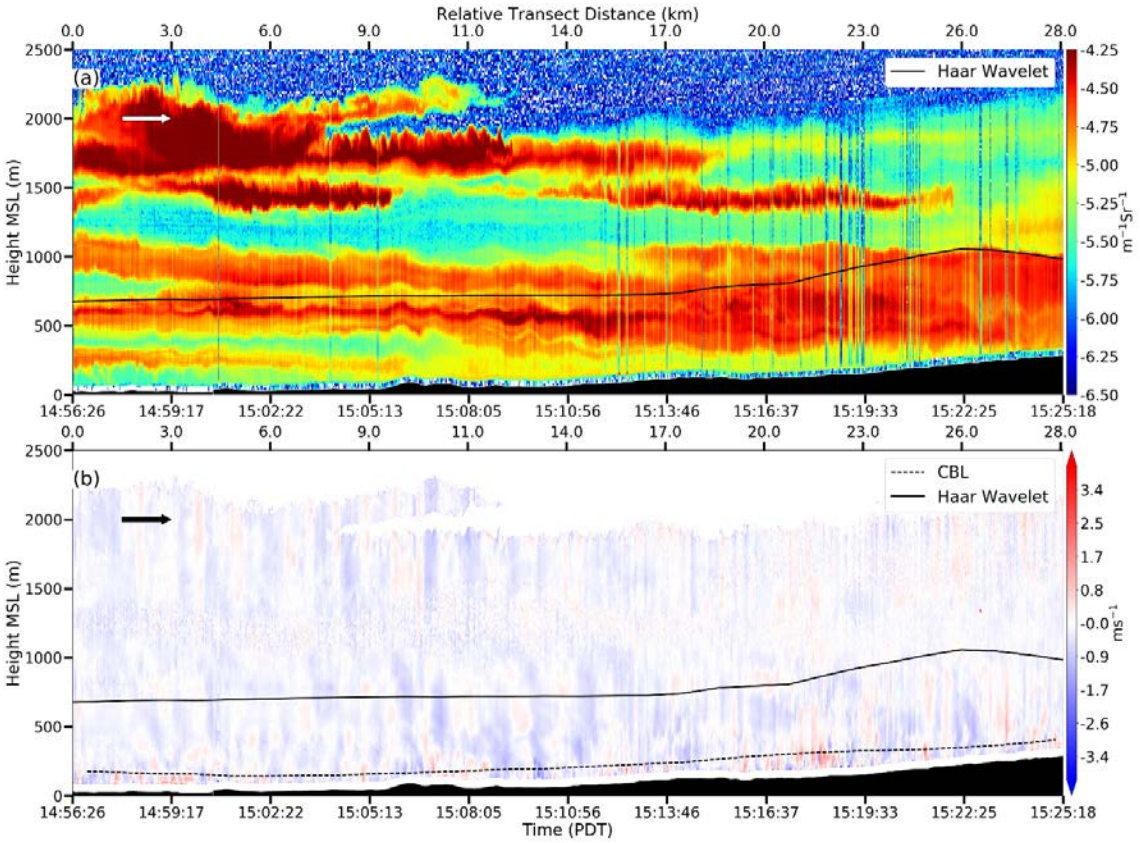

Fig. 28. As Figs. 25 and 26, but with profiles of backscatter (a) and vertical velocities (b) through the Carmel Valley.

Multiple stratified smoke layers were observed over the Carmel Valley (e.g. 300 m, 600m, 1000 m, 1500 m, and 2000 m MSL). The stratification was likely the result of stacked stable layers, potentially formed through radiation absorption in the smoke layer. No thermodynamic profiles were available to verify the presence of these stable layers, so further investigation with numerical modeling is needed to verify this hypothesis. A radiosonde was not launched in the Carmel Valley due CSU-MAPS's close proximity to the fire. A radiosonde launch from the Carmel Valley would have imposed a safety hazard for incident-related aircraft (e.g. fire-suppressing helicopters and fixed-wing aircraft). These stratified layers remain separated through the first 9 km of the transect, past which the layers below 1000 m MSL mixed. Visible gaps in backscatter returns started appearing shortly past 11 km into the valley, and were the result of the LiDAR attenuating off tree overhang.

Vertical motions in the Carmel Valley (Fig. 28b) were largely suppressed compared to the vertical motions in the Salinas and Santa Clara valleys. The average vertical velocity measured -0.15 m s^{-1} with a standard deviation of 0.33 m s^{-1}. Further breaking down into the average velocity of an updraft (downdraft), the average updraft (downdraft) was 0.21m s^{-1} (-0.26 m s^{-1}). Very few thermals formed near the surface in the valley, and any that developed were shallow. The most active thermals observed in the transect were recorded around 1515 PDT, 20 km into the transect. The primary updraft core from one thermal in this region extended 208 m AGL. The limited development of thermals is reflected in the estimated CBL heights from the vertical velocity variance analysis, with an average depth of 140 m AGL. The Haar Wavelet

analysis grossly overestimated the CBL, placing the depth of the CBL around 670 m AGL, 530 m deeper than vertical velocity variance analysis. The overestimation was caused by the stronger backscatter returns observed within the elevated smoke layers compared to the backscatter returns observed near the surface. While the Haar wavelet analysis performed well in traditional boundary layer conditions (i.e. conditions with high aerosol loading in the PBL with a sharp transition to low aerosol loading in the free atmosphere), the analysis did not natively perform well in unique cases where multiple ALs exist in the vertical. Improving the algorithm's accuracy in estimating the CBL in the Carmel Valley transect may prove difficult, as there is great ambiguity in discerning the top of the AL associated with the CBL.

4. Discussion

The bulk of this paper thus far has focused on the comparison of CBL estimates between the vertical velocity variance and backscatter analyses over multiple transects. While these transects allow for the comparison of the CBL against various regions and times in California, the transects also allow for detailed observations of various atmospheric phenomena which may not be observed by a stationary profiling instrument.

The structure of the AL over the Bay Area (Figs. 12a, 12c, 13a, 13c, 14a, 14c) varied from each transect, with certain transects exhibiting more complex ALs (e.g. Fig. 12a). While each transect displayed its own set of unique characteristics, the transects also exhibit multiple similarities. For instance, the transects show the AL rarely exceeded 600 m MSL over the Santa Clara Valley, and the greatest backscatter intensity along the Bay Area transect was generally observed within the valley. Every afternoon Bay Area transect showed evidence of a hydraulic jump while driving over the valley ridge (Mission Pass). These hydraulic jumps are particularly evident in the backscatter profiles (see Fig. 13a, 98-110 km RTD; Fig. 13c, 98-110 km RTD; 14c, 98-110 km RTD), and are associated with a sharp decrease in the depth of the AL while crossing over Mission Pass (110 km RTD). The hydraulic jump observed on 24 Aug 2016 (Fig. 13a, 98-110 km RTD) was the least pronounced, with the AL only decreasing by 100 m. The jump observed on 10 Sep 2016 (Fig. 13c, 98-110 km RTD) was more evident, with the AL decreasing by nearly 200 m. In addition, the elevated AL located at 900 m MSL showed wave structures aloft over the region of the hydraulic jump. The most pronounced hydraulic jump was observed during the early evening of 23 Sep 2016 (Fig. 14c, 98-110

km RTD). During this transect, the hydraulic jump largely suppressed the AL to ~100 m AGL. The hydraulic jumps mix clean air aloft towards the surface and can reduce the aerosol loading in the PBL.

In addition to the afternoon hydraulic jumps, the general structure of the AL past the Santa Clara Valley towards Vacaville is similar throughout the Bay Area transects. The influence of clean marine air passing through the Carquinez Strait on the AL is evident. Aerosol loading in the PBL tends to decrease in proximity to the Strait (e.g. Fig. 12a, 80-117 km RTD). The one notable exception was the Bay Area transect on 10 Sep 2016 (Fig. 13c), where the aerosol loading in the PBL remained nearly constant throughout the transect. In addition to the marine air influencing the aerosol loading, the marine influence is also associated with cold air advection (Bianco et al., 2011) and can limit the depth of the CBL.

The comparison between the Bay Area and Central Valley transects (Figs. 15, 16, 17) shows differences in the overall structure of the AL. The AL within the Central Valley (see Figs. 15a, 15c, 16a, 16c, 17a, 17c) was more consistent than compared to the Bay Area, with very few instances of light aerosol loading in the PBL. In addition, the depth of the AL in the Central Valley during the majority of the transects was nearly double compared to the Bay Area, with the exception of the morning Central Valley transect on 23 Sep 2016 (Fig. 17a). Under certain conditions, the deep AL over the Central Valley can be advected over the Bay Area, as was observed in the Bay Area transect on 9 Sep 2016 (Fig. 12c).

The complexity of the AL over the Central Valley was also variable. For instance, the AL observed during the Central Valley transect on 9 Sep 2016 (Fig. 16a) showed an AL extending to 1300 m MSL with several stratified layers around 500 m MSL, 780 m MSL, and 1100 m MSL (see Fig. 16a, 0-24 km RTD). In contrast, the afternoon Central Valley transect on the afternoon of 23 Sep 2016 (Fig. 17c) showed strong backscatter returns below 1000 m MSL, with a sharp dissipation of returns in the free atmosphere.

The structure of the AL over the Sierra Nevada was arguably dependent on the aerosol loading in the foothills of the Sierra Nevada. Sierra Nevada transects with light backscatter returns observed over the mountain, such as on 24 Aug (Fig. 6b) and the morning of 23 Sep (Fig. 20a), had light backscatter returns over the Sierra Nevada foothills. In contrast, the Sierra Nevada transects on 22 Aug (Fig. 19a), 9 Sep 2016 (Fig. 19c), and 10 Sep (Fig. 19e) showed a well-defined AL over the Sierra Nevada foothills, as well as over the Sierra crest. This suggests the primary mechanism for the development of an AL over the Sierra Nevada is the plain-mountain wind circulation. The plain-mountain wind circulation likely advects aerosols from the Central Valley up the slope of the Sierra Nevada, which has been observed in other mountainous regions (De Wekker and Kossmann, 2015). The return flow of this circulation was likely observed on 10 Sep (Fig. 19e, 156-122 km RTD). A clear example of the aerosol transport from the Central Valley along the Sierra Nevada are from the transect profiles gathered during the morning and afternoon of 23 Sep 2016 (Figs. 20a, 20b). Very limited returns were observed over the western slope during the morning compared to the

afternoon. The backscatter intensity was greatest in the foothills (Fig. 20b, 175-158 km RTD), and gradually tapered off toward Donner Summit (65 km RTD).

The structure of the CBL compared to the AL over the Sierra Nevada can be slightly different (Fig. 19). While the depth of the AL was similar in depth to the CBL over the Sierra Nevada for most of the transects, there were several instances where the depth between the two were not equivalent (see Fig. 19b, 35-53 km RTD). The vertical velocities within the CBL also varied with altitude along the Sierra Nevada. The Sierra Nevada transects on 22 Aug (Fig. 19b) and 9 Sep (Fig. 19d) displayed enhanced vertical velocities around 2000 m MSL, and was associated with an increase in the CBL depth. The cause of these enhanced vertical velocities was likely due to the enhanced sensible heat flux associated with the coniferous belt.

The transect near the Soberanes fire on 26 July 2016 (Figs. 26, 27, 28) allowed for novel mobile observations on the CBL variability in areas inundated with smoke. The transect showed shallower CBL heights associated with regions of greater quantities of smoke. The smoke layer observed over the Santa Clara Valley (Fig. 26) had lower backscatter intensity and a deeper CBL compared to the Salinas and Carmel Valleys. The transect in the Carmel Valley showed the highest amount of backscatter intensity, with a largely suppressed CBL (<135 m AGL). Further investigation with numerical modeling would provide more insight on the impact that elevated smoke layers have on CBL growth.

Under optimal atmospheric conditions (i.e. a well-defined AL and clean air aloft), the four analyses used to estimate the CBL (the vertical velocity variance, the Haar wavelet

covariance, backscatter gradient, backscatter variance) yield similar results. The analyses are limited by the atmosphere, however, as all analyses are dependent on aerosol returns. Various transects observed clean air within the PBL with elevated ALs aloft. Under these conditions, the backscatter analyses can misidentify the top of the CBL as the height of the elevated AL. The backscatter analyses largely depend on a continuous AL, and a highly variable AL can lead to errors in the analyses. The vertical velocity variance analysis outperforms the backscatter analyses under conditions with an ambiguous AL.

While the vertical velocity variance analysis can outperform the backscatter analyses, the vertical velocity analysis is not without errors. The largest limitation to the analysis is the dependence on the predefined variance threshold. The series of transects over California show there is not an all-encompassing threshold value. The 0.15 m s^{-2} variance threshold works well over regions with average updrafts greater than 1 m s^{-1} (such as over the Sierra Nevada on 22 Aug), but underestimate the CBL with average updrafts less than 1 m s^{-1} (such as in the Santa Clara Valley on 9 Sep 2016). Reducing the variance threshold improves the CBL estimate, but also leads to the analysis detecting gravity waves in ALs above the PBL. Improving CBL estimates using the vertical velocity variance may require a threshold that changes with respect to the sampling region.

While CSU-MAPS is a viable platform to study the CBL spatial variability along a transect, there is room for improvement with the correction procedures in this study. The most critical correction that needs improvement is accounting for CSU-MAPS's velocity when traveling. The transects discussed in this study were not corrected for the

horizontal projection of CSU-MAPS's velocity into the vertical. In addition, current correction procedures do not consider the contamination of strong cross winds into the vertical. To address this issue, one possible solution is to alter the LiDAR scanning routine to allow for the collection of vertical wind profiles while driving. Another area for improvement relates to the tilt correction of the vertical velocities. The current procedure only calculates the vertical component of the tilted radial velocity vector, which is not the true vertical velocity vector. More sophisticated correction techniques such as those discussed in Hill et al. (2008), which also account for the angular momentum of a platform, may help improve the vertical velocity estimate.

5. Summary and Conclusions

A series of cross-California transects were conducted from August – September 2016. A truck-mounted Doppler LiDAR was used to obtain vertical profiles of the backscatter intensity and radial velocity. With the backscatter profiles, three different methods were used to estimate the CBL, including the vertical backscatter gradient, the backscatter variance, and the Haar wavelet covariance. The CBL was also estimated using the vertical velocity variance. Key findings from the transects include:

- Mobile Doppler LiDAR profiles provide unique and detailed observations of the spatial variability of the AL and CBL. In addition, the mobile platform allows for observations of atmospheric phenomena over California, including observations of aerosol transport along the Sierra Nevada.
- Comparison of stationary and mobile data show distortion in the apparent width of a thermal, with thermals appearing more narrow while mobile. The overall distribution is similar, but the mobile data has a negative bias compared to the stationary data. In addition, the vertical velocity variance and skewness profiles slightly vary in structure, which may be the result of the increased number of thermals sampled while mobile.
- Composite variance profiles between the transects show similar profiles to those reported in Weissmann et al. (2005), with the variance exhibiting a negative trend in height. The composite skewness profile for the Central Valley transect showed the profile increasing in skewness with height, and peaking within the upper third of the CBL.

- The CBL backscatter analyses are extremely dependent on a strong, and well-defined AL. When mobile, this AL may be highly variable and can lead to errors in CBL estimates. This is particularly true when aerosol loading in the PBL is sparse and an elevated AL is present.

- The vertical velocity variance analysis can yield better estimates of the CBL compared to the backscatter analyses in conditions with ambiguous ALs, but the accuracy is dependent on the specified variance threshold. A lower variance threshold can yield improved estimates of the CBL under conditions with updraft velocities between ± 1 m s^{-1}, but can also lead to overestimations due to the detection of gravity waves.

In addition to the California transects, mobile transects were conducted down-wind of the Soberanes Fire. The smoke layer over the Santa Clara and Salinas Valleys had estimated AOT of 0.5 and close to 1, respectively. The Carmel Valley arguably had the highest AOT, but no estimate was available due to MODIS misidentifying the smoke layer as a cloud. The profiles from the transects show:

- The CBL depth decreases as the aerosol loading associated with the smoke layer increases. The CBL was deepest in the Santa Clara Valley (201 m AGL), and was shallower in the Salinas Valley (151 m AGL). Very few thermals were observed in the Carmel Valley, and the CBL was largely suppressed (<135 m AGL).

- The Haar wavelet analysis loses accuracy in the Carmel Valley due to the complex AL structures. The analysis overestimated the CBL due to several stratified ALs with enhanced backscatter returns, and relatively light aerosol loading near the surface.

In summary, the mobile Doppler LiDAR mesurements provide detailed spatially resolved observations of the CBL. The CBL determination methods, particularly the Haar wavelet covariance and the vertical velocity variance, yield good estimates of the CBL under optimal atmospheric conditions (high aerosol loading in the PBL with clean air in the free-atmosphere). The performance of the backscatter analyses degraded under conditions with light aerosol loading near the surface with elevated ALs. Errors may also potentially arise in the vertical velocity variance analysis due to the contamination of horizontal winds into the vertical (either induced from truck motion or ambient background winds). Contamination of horizontal winds into the vertical is not an issue with a perfectly level instrument, but CSU-MAPS is seldom level when in motion.

While the transects provided detailed observations of the vertical velocity, the transects lacked thermodynamic observations. The addition of a microwave temperature profile, which can be mounted on CSU-MAPS (Clements and Oliphant, 2014), would provide these data. In addition to adding a microwave profiler, the scanning procedure could be modified to obtain wind profiles while mobile. The wind profiles would further help correct the mobile data, and might prevent artifacts from developing at higher elevations when correction for truck motion.

The overall structure of the transects also limits detailed observations of atmospheric phenomena, such as aerosol transport from the Central Valley to the Sierra Nevada. Future research could focus more on these phenomena, with transects focusing on smaller portions of California to provide more detailed temporal observations of the phenomena.

References

Banta, R. M., 1984: Daytime boundary-layer evolution over mountainous terrain. Part I: Observations of dry circulations. *Mon. Weather Rev.* **112**, 340-356.

Banta, R. M., P. B. Shepson, J. W. Bottenheim, K. G. Anlauf, H. A. Wiebe, A. Gallant, T. Biesenthal, L. D. Olivier, C.-J. Zhu, I. G. McKendry, D. G. Steyn, 1997: Nocturnal cleansing flows in a tributary valley. *Atmos. Environ.* **31**, 2147-2162. doi: 10.1016/S1352-2310(96)00359-7.

Banta, R. M., Y. L. Pichugina, W. A. Brewer, 2006: Turbulent velocity variance profiles in the stable boundary layer generated by a nocturnal low-level jet. *J. Atmos. Sci.* **63**, 2700-2719. doi:10.1175/JAS3776.1.

Beyrich, F., 1995: Mixing-height estimation in the convective boundary layer using sodar data. *Bound. Layer Meteorol.* **74**, 1-18.

Bianco, L., I. V. Djalalova, C. W. King, J. M. Wilczak, 2011: Diurnal evolution and annual variability of boundary-layer height and its correlation to other meteorological variables in California's Central Valley. *Bound. Layer Meteorol.* **140**, 491-511. doi:10.1007/s10546-011-9622-4.

Bosart, B. L., W.-C. Lee, and R. M. Wakimoto, 2002: Procedures to improve the accuracy of airborne Doppler radar data. *J. Atmos. Oceanic Technol.* **19**, 322-339.

Bozier, K. E., G. N. Pearson, and G. C. Collier, 2007: Doppler lidar observations of Russian forest fire plumes over Helsinki. *Weather* **68**, 204-208.

Carroll, J. J., 1989: Analysis of airborne Doppler lidar measurements of the extended California sea breeze. *J. Atmos. Oceanic Technol.* **6**, 820-831.

Clements, C. B., and A. J. Oliphant, 2014: The California state university mobile atmospheric profiling system: a facility for research and education in boundary layer meteorology. *Bull. Amer. Meteorol. Soc.* **95**, 1713-1724. doi:10.1017/BAMS-D-13-00179.1.

Crescenti, G. H., 1998: The degradation of Doppler sodar performance due to noise: a review. *Atmos. Environ.* **32**, 1499-1509.

Dai, C., Q. Wang, J. A. Kalogiros, D. H. Lenschow, Z. Gao, and M. Zhou, 2014: Determining boundary-layer height from aircraft measurements. *Bound. Layer. Meteorol.* **152**, 277-302. doi:10.1007/s10546-014-9929-z.

De Wekker, S. F. J., D. G. Steyn, and S. Nyeki, 2004: A comparison of aerosol-layer and convective boundary layer structure over a mountain range during STAAARTE ’97. *Bound. Layer Meteorol.* **113**, 249-271.

De Wekker, S. F. J., K. S. Godwin, G. D. Emmitt, and S. Greco, 2012: Airborne Doppler lidar measurements of valley flows in complex coastal terrain. *J. Appl. Meteorol. Clim.* **51**, 1558-1574. doi:10.1175/JAMC-D-10-05034.1.

De Wekker, S. F. J. and M. Kossmann, 2015: Convective Boundary Layer Heights Over Mountainous Terrain – A Review of Concepts. *Front. Earth. Sci.* **3**, 77.

Endlich, R. M., F. L. Ludwig, E. E. Uthe, 1979: An automatic method for determining the mixing deoth from lidar observations. *Atmos. Environ.* **13**, 1051-1056.

Hill, R. J., W. A. Brewer, and S. C. Tucker, 2008: Platform-motion correction of velocity measured by Doppler lidar. *J. Atmos. Oceanic Technol.* **25**, 1369-1382. doi:10.1175/2007JTECHA972.1.

Hogan, R. J., A. L. M. Grant, A. J. Illingworth, G.N. Pearson, and E.J. O’Connor, 2009: Vertical velocity variance and skewness in clear and cloud-topped boundary layers as revealed by Doppler Lidar. *Q.J.R. Meteorol. Soc.* **135**, 635-643.

Hooper, W. P., and E. W. Eloranta, 1986: Lidar Measurements of wind in the planetary boundary layer: the method, accuracy and results from joint measurements with radiosonde and kytoon. *J. Clim. Appl. Meteorol.* **25**, 990-1001.

Kossmann, M., R. Vögtlin, U. Corsmeier, B. Vogel, F. Fiedler, H.-J. Binder, N. Kalthoff, and F.Beyrich, 1998: Aspects of the convective boundary layer structure over complex terrain. *Atmos. Environ.* **32**, 1323-1348.

Lareau, N. P., C. B. Clements, 2015: Cold smoke: smoke-induced density currents cause unexpected smoke transport near large wildfires. *Atmos. Chem. Phys.* **15**, 11513-11520. doi:10.5194/acp-15-11503-2015.

Lee, W.-C., P. Dodge, F. D. Marks, and P. H. Hildebrand, 1994: Mapping of airborne Doppler radar data. *J. Atmos. Oceanic Technol.* **11**, 572-578.

Lee, X., and T. A. Black, 1993: Atmospheric turbulence within and above a douglass-fir stand. Part II: eddy fluxes of sensible heat and water vapour. *Bound. Layer Meteorol.* **64**, 369-389.

Lenschow, D. H., J. C. Wyngaard, and W. T. Pennell, 1980: Mean-field and second-momentum budgets in a baroclinic, convective boundary layer. *J. Atmos. Sci.* **37**, 1313-1326.

Melfi, S.H., J.D. Spinhirne, S-H. Chou, and S. P. Palm, 1985: Lidar observations of vertically organized convection in the planetary boundary layer over the ocean. *J. Clim. Appl. Meteorol.* **24**, 806-821.

Menut, L., C. Flamant, J. Pelon, and P. H. Flamant, 1999: Urban boundary-layer height determination from lidar measurements over the Paris area. *Appl. Opt.* **38**, 945-954.

McElroy, J. L. and T.B. Smith, 1991: Lidar decriptions of mixing-layer thickness characteristics in a complex terrain/coastal environment. *J. Appl. Meterol.* **30**, 585-597.

Moeng, C-H. and R. Rotunno, 1990: Vertical velocity skewness in the buoyancy-driven boundary layer. *J. Atmos. Sci.* **47** 1149–1162.

Moyer, K. A., and G. S. Young, 1991: Observations of vertical velocity skewness within the marine stratocumulus-topped boundary layer. *J. Atmos. Sci.* **48**, 403–410.

Nyeki, S., M. Kalberer, I. Colbeck, S. De Wekker, M. Furger, H. W. Gäggeler, M. Kossmann, M. Lugauer, D. Steyn, E. Weingartner, M. Wirth, and U. Baltensperger, 2000: Convective boundary layer evolution to 4 km asl over high-alpine terrain: airborne lidar observations in the alps. *Geophys. Res. Lett.* **27**, 689-692.

Nyeki, S., E. Eleftheriadis, U. Baltensperger, I. Colbeck, M. Fiebig, A. Fix, C. Kiemle, M. Lazardis, and A. Petzold, 2002: Airborne lidar and in-situ aerosol observations of an elevated layer, leeward of the European Alps and Apennines. *Geophys. Res. Lett.* **29**, 33. doi:10.129/2002GL014897.

Pearson, G., F. Davies, C. Collier, 2009: An analysis of the performace of the UFAM pulsed Doppler lidar for observing the boundary layer. *J. Atmos. Oceanic Technol.* **26**, 240-250. doi:10.1175/2008JTECHA1128.1.

Piironen, A. K., E. W. Eloranta, 1995: Convective boundary layer mean depths and cloud geometrical properties obtained from volume imaging lidar data. *J. Geophy. Res.* **100**, 25567-25576

Poulos, G. S., W. Blumen, D. C. Fritts, J. K. Lundquist, J. Sun, S. P. Burns, C. Nappo, R. Banta, R. Newsom, J. Cuxart, E. Terradellas, B. Balsley, and M. Jensen, 2002: CASES-99: a comprehensive investigation of the stable nocturnal boundary layer. *Bull. Am. Meteorol. Soc.* **83**, 55-581.

Reitebuch, O., H. Volkert, C. Werner, A. Dabas, P.Delville, P. Drobinski, P. H. Flamant, and E. Richard, 2003: Determination of airflow across the Alpine ridge by a combination of airborne Doppler lidar, routine radiosounding, and numerical simulation. *Q. J. R. Meteorol. Soc.* **129**, 715-727. doi:10.1256/qj.02.42.

Reuten, C., D. G. Steyn, K. B. Strawbridge, and P. Bovis, 2005: Observations of the relation between upslope flows and the convective boundary layer in steep terrain. *Bound. Layer Meterol.* **116**, 37-61. doi:10.1007/s10546-004-7299-7.

Robock, A., 1988: Enhancement of surface cooling due to forest fire smoke. *Science* **242**, 911-913.

Saiki, E. M., C.-H. Moeng, and P. P. Sullivan, 2000: Large-eddy simulation of the stably stratified planetary boundary layer. *Bound. Layer Meteorol.* **95**, 1-30.

Seibert, P., F. Beyrich, S.-E. Gryning, S. Joffre, A. Rasmussen, P. Tercier, 2000: Review and intercomparison of operational methods for the determination of the mixing height. *Atmos. Environ.* **34**, 1001-1027.

Sellers, P.J., F.G. Hall, R. D. Kelly, A. Black, D. Baldocci, J. Berry, M. Ryan, K. J. Ranson, P. M. Crill, D. P. Lettenmaier, H. Margolis, J. Cihlar, J. Newcomer, D. Fitziarrald, P.G. Jarvis, S. T. Gower, D. Halliwell, D. Williams, B. Goodison, D. E. Wickland, and F. E. Guertin, 1997: Experiment overview, scientific results, and future directions. *J. Geophys. Res.* **102**, 28731-28769.

Stull, R. B., 1988: *An introduction to Boundary Layer Meteorology*. Dordrecht: Kluwer Academic Publishers.

Tucker, S. C., W. A. Brewer, R. M. Banta, C. J. Senff, S. P. Sanberg, D. C. Law, A. M. Weickmann, and R. M. Hardesty. Doppler lidar estimation of mixing height using turbulence, shear, and aerosol profiles, 2009: *J. Atmos. Oceanic Technol.* **26**, 673-688. doi:101175/2008JTECHA1157.1.

Wang, J., and S. A. Christopher, 2006: Mesoscale modeling of Central American smoke transport to the United States: 2. Smoke radiative impact on regional surface energy budget and boundary layer evolution. *J. Geophys. Res.* **111**, D14S92. doi:10.1029/2005JD006720.

Ware, J., E. A. Kort, P. DeCola,, and R. Duren, 2016: Aerosol lidar observations of atmospheric mixing in Los Angeles: climatology and implications for greenhouse gas observations. *J. Geophys. Res. Atmos.* **121**. doi:10.1002/2016JD024953.

Weissmann, W., F. J. Braun, L. Ganter, G. J. Mayr, S. Rahm, and O. Reitebuch, 2005: The alpine mountain-plain circulation: Airborne Doppler lidar measurements and numerical simulations. *Mon. Weather Rev.* **133**, 3095-3109.

Webster, P.J., and R. Lukas, 1992: TOGA COARE: the coupled ocean atmosphere response experiment *Bull Am. Meteorol. Soc.* **73**, 1377-1416.